MASSACHUSETTS INSTITUTE OF TECHNOLOGY

APOLLO

GUIDANCE, NAVIGATION AND CONTROL

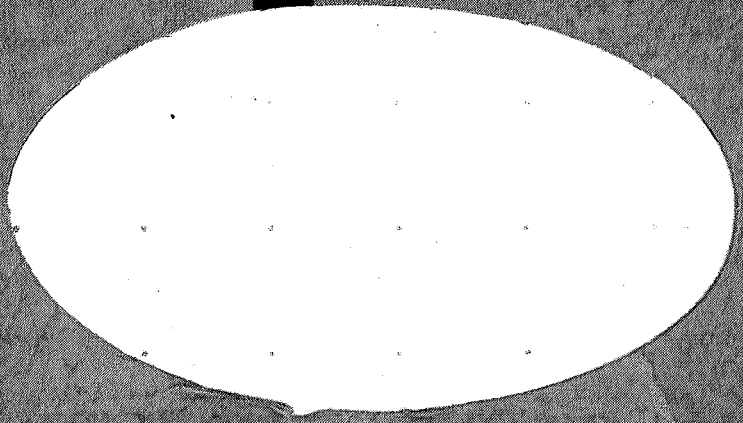

MIT CHARLES STARK DRAPER LABORATORY

CAMBRIDGE MASSACHUSETTS 02139

MASSACHUSETTS INSTITUTE OF TECHNOLOGY

GUIDANCE, NAVIGATION AND CONTROL

Approved: Glenn Ogletree Date: 5 October 1971
G. OGLETREE, DIRECTOR, NAVIGATION SUBSYSTEMS
APOLLO GUIDANCE AND NAVIGATION PROGRAM

Approved: N E Sears Date: Oct 6, 1971
N. E. SEARS, DIRECTOR, G&N SYSTEMS
APOLLO GUIDANCE AND NAVIGATION PROGRAM

Approved: R R Ragan 1 for Date: 7 Oct 71
D. G. HOAG, DIRECTOR
APOLLO GUIDANCE AND NAVIGATION PROGRAM

Approved: Ralph R Ragan Date: 7 Oct 71
R. R. RAGAN, DEPUTY DIRECTOR
CHARLES STARK DRAPER LABORATORY

E-2606

SPACE SHUTTLE VEHICLE AUTOMATIC DOCKING STUDY FINAL REPORT

by

Earle P. Blanchard
Richard C. Hutchinson
Leonard B. Johnson

OCTOBER 1971

MIT CHARLES STARK DRAPER LABORATORY
CAMBRIDGE, MASSACHUSETTS, 02139

ACKNOWLEDGEMENT

This report was prepared under DSR Project 55-40800, sponsored by the Manned Spacecraft Center of the National Aeronautics and Space Administration through Contract NAS 9-10268.

The authors thank the following individuals for their contributions during the tenure of this program.

Orin Anderson and James Deckert for their respective studies involving Kalman filtering, Thomas Gaul for his support in the development of the guidance equations and Mrs. Katherine Tompkins for her careful construction of the computer routines which constitute the implemented portion of the computer simulation.

We are also grateful to the other persons too numerous to mention who made necessary contributions to this effort.

Abstract

The material presented herein is divided into three main areas of accomplishment. The first is a description of the Angle Only Docking Sensor concept and the computational requirements to develop useful guidance information from the raw angle only data. The second describes the analytical effort including the MIT in-house computer simulation, the development of guidance equations and vehicle stability related thereto, and presents the results of studies covering the effects of employing Kalman filtering with the sensor under study. The third area presents the conclusions and recommendations resulting from the program.

Much of the material herein has appeared in previous reports, but is included here for the sake of completeness. Section 1.1 includes new material indicating how the computer might operate to identify the individual sources in the target array. The guidance equations developed in Section 2.2 represent the most significant increase in new material. Other more recently acquired information is included in the various related sections.

Outline

Tables

List of Illustrations

AUTOMATIC DOCKING STUDY

Final Report

1.0 The Angle Only Docking Sensor Concept

1.1 Sensor Sub-System Description

This automatic docking system embodies a sensor configuration which measures line-of-sight angles to energy reflectors, backscatterers or sources (hereafter called sources) uniquely mounted on another vehicle such as a space station (hereafter called the subject). A priori knowledge of the location of the sources on the subject is required. The line-of-sight data is processed by special computation to develop range and attitude information which may be used directly with a guidance or monitoring system. Range-rate, attitude-rate, and other pertinent parameters of dynamic geometry necessary for specific applications can be developed from the measured and computed data of this system.

Because the measurement technique requires only angle information, the hardware implementation of the sensor is expected to possess the advantages of simplicity, reliability, low weight and low power consumption. This measurement technique also provides the desirable characteristic of more accurate solutions for range as the range to the subject is decreased. It is ideally suited for application in the docking of spacecraft, or for stationkeeping between two vehicles in space. It further can be used during rendezvous and for horizon and star sightings.

Figure 1 shows the geometry which exists between the sensor and the target. Positions 1, 2, 3, and 4 are the locations of the sources in three dimensional space. The vectors $\bar{R}_{12}$, $\bar{R}_{13}$, $\bar{R}_{14}$,

Figure 1

SENSOR- SUBJECT GEOMETRY

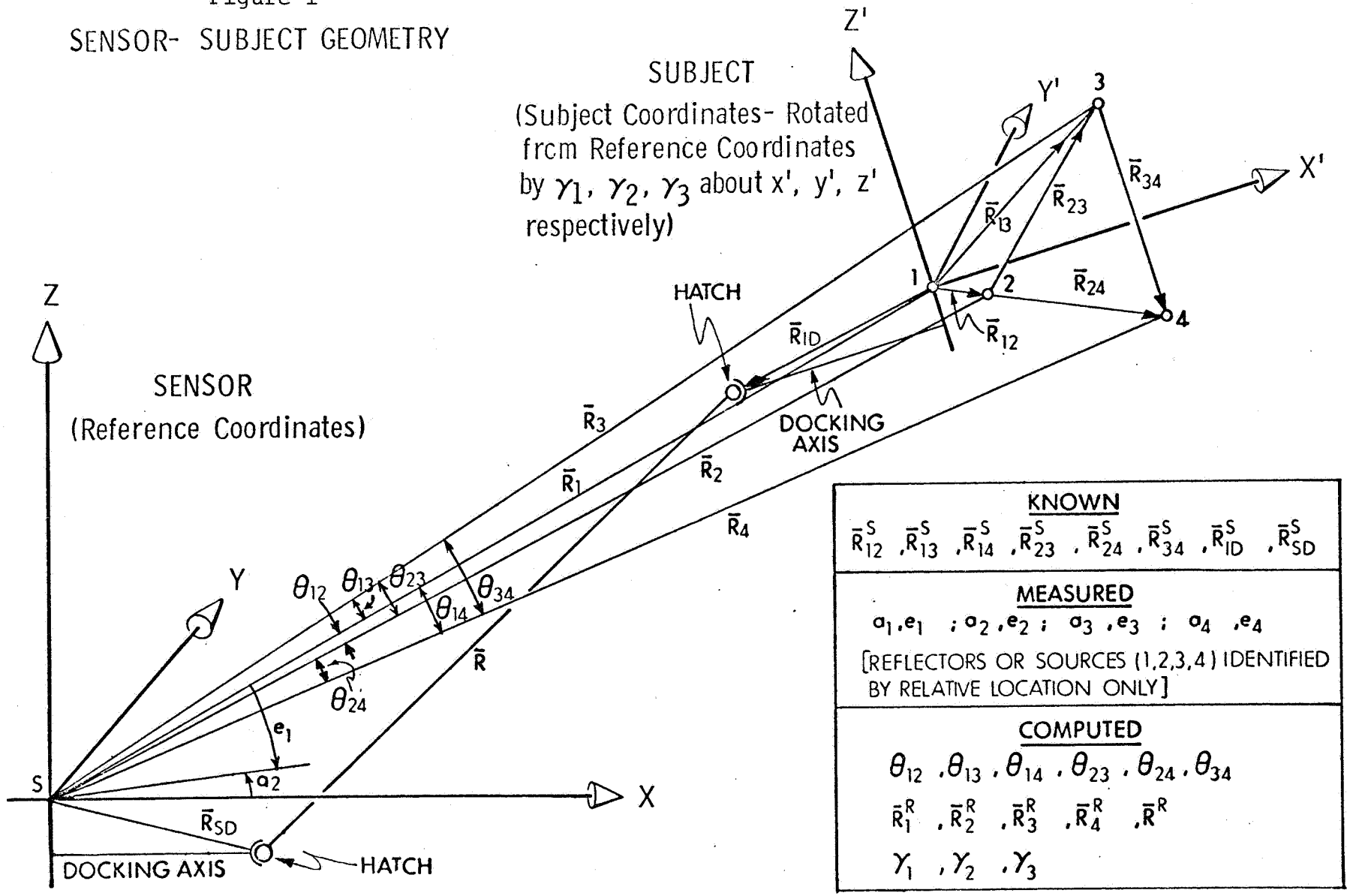

KNOWN

$\bar{R}_{12}^S$, $\bar{R}_{13}^S$, $\bar{R}_{14}^S$, $\bar{R}_{23}^S$, $\bar{R}_{24}^S$, $\bar{R}_{34}^S$, $\bar{R}_{ID}^S$, $\bar{R}_{SD}^S$

MEASURED

a_1, e_1 ; a_2, e_2 ; a_3, e_3 ; a_4, e_4

[REFLECTORS OR SOURCES (1,2,3,4) IDENTIFIED BY RELATIVE LOCATION ONLY]

COMPUTED

θ_{12} , θ_{13} , θ_{14} , θ_{23} , θ_{24} , θ_{34}

$\bar{R}_1^R$, $\bar{R}_2^R$, $\bar{R}_3^R$, $\bar{R}_4^R$, $\bar{R}^R$

γ_1 , γ_2 , γ_3

SUPERSCRIPTS

R - REFERENCE COORDINATES
S - SUBJECT COORDINATES

DOCKING AXES ARE DISPLACED FROM AND PARALLEL TO THEIR RESPECTIVE X-AXES

$\bar{R}_{23}$, $\bar{R}_{24}$, and $\bar{R}_{34}$ are shown in the subject coordinate system between the sources and are pre-determined by design (see Figure 2). The sensor measures the azimuth and elevation angles (a_i, e_i) to each source and passes this information to a computer. Associated with each set of azimuth and elevation angles, e.g., with a_3, e_3, is a line-of-sight between the origin of the sensor reference coordinate system and the particular source. The lines-of-sight together with the vectors $\bar{R}_{12}$, $\bar{R}_{13}$, etc. form triangles with a common vertex point at the origin of the sensor reference coordinate system. The computer functions to calculate the lengths of these lines-of-sight based on the vectors defining the source locations and the measured angles (a_i, e_i).

Ambiguities can exist when the sensor is required to operate from all directions relative to the subject (4π steradian coverage). Under most circumstances the computer can develop unique solutions for the range to each source; however, the amount of computation and comparison required to obtain the solution becomes prohibitive.

Analysis has shown that the volume of computational trial and error can be reduced considerably if system operating limits are defined and known, and the source configuration is designed to permit recognition of one source by its angular position relative to the other sources under all allowed attitude relationships between source and subject within the defined operating limits. See Figure 3. Hence, it is not required that the sources be individually identified by the sensor, i.e., the system does not require that its sensor portion distinguish and relate a given source with its associated azimuth angle, elevation angle and line-of-sight. An intrinsic advantage of

Figure 2

SOURCE/REFLECTOR CONFIGURATION (SUBJECT COORDINATES)

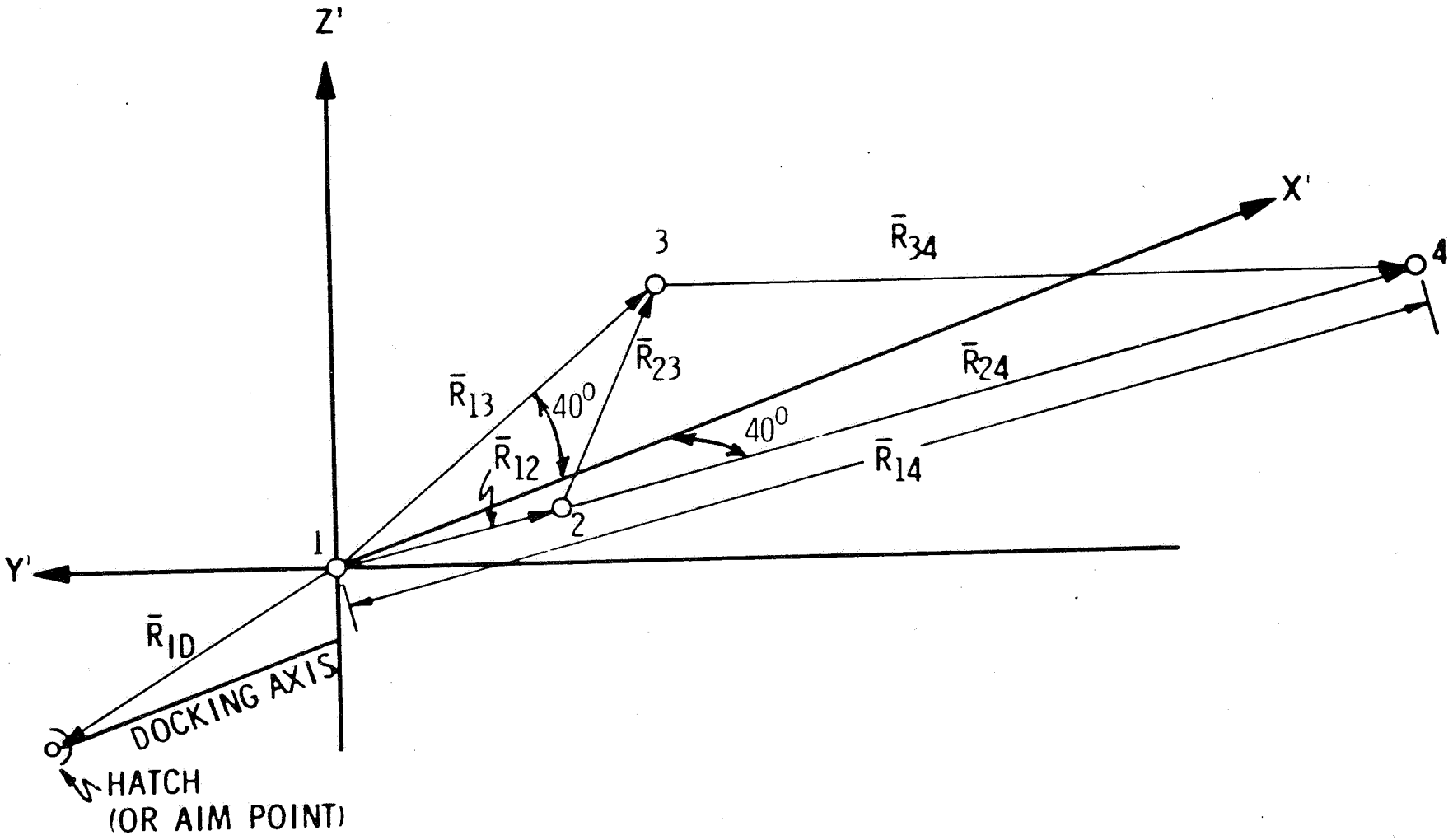

Figure 3

APPEARANCE OF SOURCES vs. ATTITUDE OF CONFIGURATION IN SENSOR COORDINATES

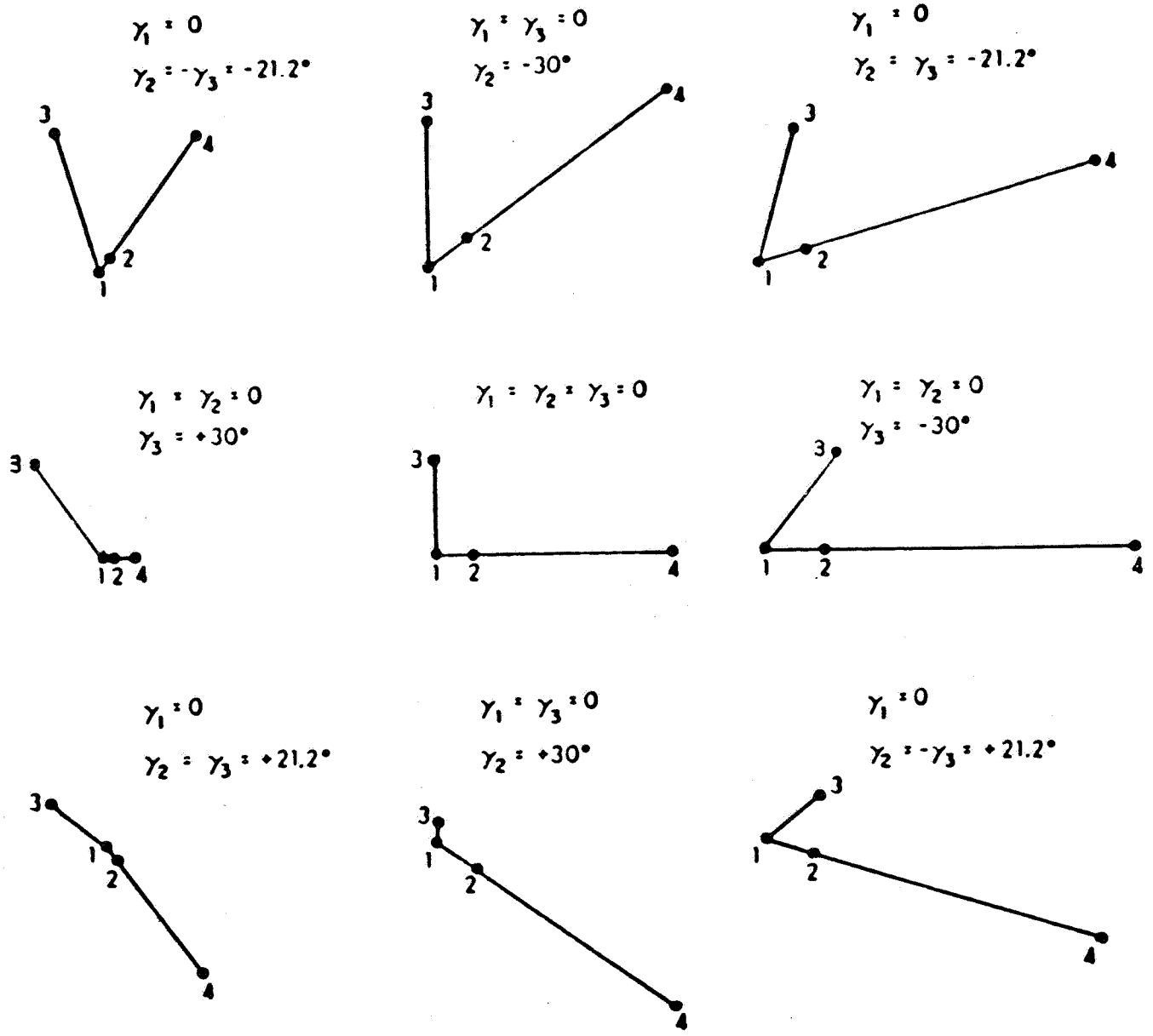

this system is its ability to compute relative distance, velocity and attitude, without the necessity of signature information from the individual sources. Figure 4 presents a logic procedure by which the computer is enabled to identify the specific sources.

The computer initiates its calculating process by selecting three of the four possible lines-of-sight along with three source position vectors, and three sets of measured azimuth and elevation angles. At long ranges, the first set of three sources includes the three sources at the extremities of the source configuration simply to yield greater accuracy to the solutions. For close ranges, the computer drops the most extreme source and replaces it with the remaining source closer to the subject coordinate origin. The computer then increments through the three equations corresponding to the remaining sources and develops solutions for the range to all sources. Once the ranges to the sources have been ascertained, the computer develops a transfer matrix describing the orientation between the sensor and subject coordinate system. The matrix then provides the means of determining the existing Euler angles between vehicles and the subsequent solution for the range between docking hatches. Relative velocity and angle rates are then derived by averaging the difference between consecutive solutions for position and angle.

There are several hardware configuration options for the sensor as well as mathematical procedures for solving the associated geometry. The source or reflector configuration may also have many forms depending upon the desired operational limits of range and aspect angle between sensor and subject.

Figure 4

SOURCE IDENTIFICATION PROCEDURE

Read y, z coordinates for each source/reflector return.

Mark A — Greatest "z" reading and corresponding "y" reading.

Mark B — Next greatest "z" reading and corresponding "y" reading.

Mark C — Next greatest "z" reading and corresponding "y" reading.

Mark D — Last "z" reading and corresponding "y" reading.

Determine Ratios:

$$\frac{z_A - z_B}{y_A - y_B} ; \frac{z_B - z_C}{y_B - y_C} ; \frac{z_C - z_D}{y_C - y_D} ; \frac{z_A - z_C}{y_A - y_C} ; \frac{z_A - z_D}{y_A - y_D} ; \frac{z_B - z_D}{y_B - y_D}$$

Select ratios which are equal to within ± 1%.

Size in descending order the Δy's for each of the equal ratios.

Invert, if necessary to make all selected individual ratios >1.

Compare ratios to 6.25 ± 0.06.

Accept ratios which fall within limits.

The line with the largest Δy of the accepted ratios is terminated by sources #1 and #4

The line with the smallest Δy of the accepted ratios is terminated by sources #1 and #2.

The common source is #1.

The extreme source is #4.

The source between is #2.

The remaining source is #3.

1.2 Sensor Configuration

For automatic docking, an important requirement for the sensor is the capability to sense the multiple sources and to measure the angles of the lines-of-sight to them simultaneously or nearly simultaneously to prevent staleness of computed data and resulting control errors.

The most feasible and readily available hardware configurations for this purpose are phototube devices. A vidicon can raster scan its entire field of view in several milliseconds and is quite suitable for the docking and stationkeeping operations. The sensor's usefulness can be increased to accomplish rendezvous and star sighting and horizon scanning by replacing the vidicon with a high gain image dissector as the heart of the sensor receiver which can also perform the docking and stationkeeping functions.

1.3 Source/Reflector Configuration

The configuration of the sources or reflectors is dependent upon many conditions:

a) the size and shape of the subject vehicle or structure,
b) interference with other equipment - either physically or by radiation,
c) the amount of spherical coverage about the subject vehicle required for sensor operation,
d) sensor field of view, resolution, and accuracy at minimum and maximum operating ranges.

Although the source arrangement can be designed to operate over a complete sphere of 4π steradians, such an operational requirement is highly unlikely and usually unnecessary in

practice. In fact, judicious choice of the angular operating region of the system results in computational simplification. This point is illustrated by the configuration of Figure 2 which assumes no conflict with conditions (a) and (b) above but which is designed to operate with a sensor always within a $\pm 30^{\circ}$ cone symmetrically oriented about the subject vehicle axis, for example, with the apex of the cone at the docking hatch. Based on this operating region, the vectors $\bar{R}_{12}$, $\bar{R}_{13}$, $\bar{R}_{14}$ have been selected to assure that the vectors between sensor and sources (Figure 1) will always satisfy the relationship $R_1 < R_2$, $R_2 < R_3$, $R_3 < R_4$. The solution for these ranges may now be obtained by computing single roots rather than all eight roots to each set of equations as described on pages 12 and 13.

Further computational simplification occurs if the individual sources are arranged to permit their unique identification within the 60° operating cone by their relative location. To illustrate this possibilty, Figure 3 shows patterns resulting from the particular choice of source locations of Figure 2 when viewed by the sensor at the center and at 8 extreme locations about the cone. Certain characteristics of the pattern persist despite subject vehicle attitude changes within the operating cone. For example, sources 1, 2, and 4 are always along a straight line with point 2 between points 1 and 4. See Figure 3. By recognizing these pattern characteristics, the need for computer guesswork in selecting the lines-of-sight to the various sources is reduced or avoided, thereby eliminating the additional computation associated with trial and error and allowing the relative geometry to be solved with only one set of equations, i.e., using only three source lines-of-sight for the solution.

Thus the configuration shown provides the sensor and its computational system with the ability to associate the proper lines-of-sight to each source and to solve for the range to each source unambiguously, within the limits of sensor angle accuracy. Again Figure 4 illustrates a possible logic procedure for source identification.

This configuration also offers another advantage to the sensor-computer system in consideration of condition (d). The lengths of $\bar{R}_{12}$, $\bar{R}_{13}$, $\bar{R}_{14}$ may be selected to allow more accurate solution at maximum ranges by choosing large distances between points 1 and 3, and 1 and 4. In a docking operation where the distance between vehicles continues to decrease after alignment and an aim point position have been achieved, the sensor-computer system can, at the proper range, drop the larger line-of-sight angle source 4 and operate with sources 1, 2, and 3, thereby reducing the sensor field of view requirement.

1.4 Computation

Several approaches for solving the geometry exist. One method is to employ vector analysis. The sensor supplies the angles (a_1, e_1; a_2, e_2; a_3, e_3; a_4, e_4) to the four sources or reflectors as shown in Figure 1. For the purpose of this example it is assumed the sensor cannot differentiate between sources, but can pair the azimuth and elevation angles properly.

Each angle existing between the lines-of-sight is computed:

$$\cos \theta_{ij} = (\text{unit } \bar{R}_i) \cdot (\text{unit } \bar{R}_j)$$

or

$$\cos \theta_{ij} = \cos a_i \cos e_i \cos a_j \cos e_j + \sin a_i \cos e_i \sin a_j \cos e_j + \sin e_i \sin e_j$$

The computer solves for the cosines of all angles between the lines-of-sight as viewed from the sensor:

$$\theta_{12},\ \theta_{13},\ \theta_{14},\ \theta_{23},\ \text{and}\ \theta_{34}$$

The equations for solution of the triangles reduce to the law of cosines:

Set I (1-2-3-1)

$$R_2 = R_1 \cos\theta_{12} \pm \sqrt{R_{12}^2 - R_1^2 (1 - \cos^2\theta_{12})}$$

$$R_3 = R_3 \cos\theta_{23} \pm \sqrt{R_{23}^2 - R_2^2 (1 - \cos^2\theta_{23})}$$

$$R_1 = R_3 \cos\theta_{13} \pm \sqrt{R_{13}^2 - R_3^2 (1 - \cos^2\theta_{13})}$$

Set II (1-3-4-1)

$$R_3 = R_1 \cos\theta_{13} \pm \sqrt{R_{13}^2 - R_1^2 (1 - \cos^2\theta_{13})}$$

$$R_4 = R_3 \cos\theta_{34} \pm \sqrt{R_{34}^2 - R_3^2 (1 - \cos^2\theta_{34})}$$

$$R_1 = R_4 \cos\theta_{14} \pm \sqrt{R_{14}^2 - R_4^2 (1 - \cos^2\theta_{14})}$$

Set III (1-2-4-1)

$$R_2 = R_1 \cos\theta_{12} \pm \sqrt{R_{12}^2 - R_2^2 (1 - \cos^2\theta_{12})}$$

$$R_4 = R_2 \cos\theta_{24} \pm \sqrt{R_{24}^2 - R_2^2 (1 - \cos^2\theta_{24})}$$

$$R_1 = R_4 \cos\theta_{14} \pm \sqrt{R_{14}^2 - R_4^2 (1 - \cos^2\theta_{14})}$$

where R_1, R_2, R_3, R_4 are the magnitudes of vectors $\bar{R}_1$, $\bar{R}_2$, $\bar{R}_3$, and $\bar{R}_4$ respectively, see Figure 1, and where R_{12}, R_{13}, R_{14}, R_{23}, R_{24}, R_{34}, are the magnitudes of vectors $\bar{R}_{12}$, $\bar{R}_{13}$, $\bar{R}_{14}$, $\bar{R}_{23}$, $\bar{R}_{24}$, $\bar{R}_{34}$ respectively. The sets of equations each have eight possible solutions. However, as noted in Section 1.3, if the sensor is located within a predetermined cone whose apex is at the subject coordinate system origin and the cone axis is coincident with the subject -X'-axis and the sources are located on the subject in a manner which causes the vectors $\bar{R}_{12}$, $\bar{R}_{13}$, $\bar{R}_{14}$, $\bar{R}_{24}$, and $\bar{R}_{34}$ to have angles with respect to the x-axis of the subject coordinate system that are less than the complement of the cone radius angle, the eight roots of each set of equations reduce to a single root in each case.

Thus with an operating cone of 60° diameter and with the source configuration vectors ($\bar{R}_{12}$, $\bar{R}_{13}$, etc) properly selected as, for example in Figure 2 where $R_1 < R_2$, $R_2 < R_3$ and $R_3 < R_4$ will always be true, the multiple roots can be eliminated simplifying the equations to:

Set I

$$R_2 = R_1 \cos\theta_{12} + \sqrt{R_{12}^2 - R_1^2 (1 - \cos^2\theta_{12})}$$

$$R_3 = R_2 \cos\theta_{23} + \sqrt{R_{23}^2 - R_2^2 (1 - \cos^2\theta_{23})}$$

$$R_1 = R_3 \cos\theta_{13} - \sqrt{R_{13}^2 - R_3^2 (1 - \cos^2\theta_{13})}$$

Set II

$$R_3 = R_1 \cos\theta_{13} + \sqrt{R_{13}^2 - R_1^2 (1 - \cos^2\theta_{13})}$$

$$R_4 = R_3 \cos\theta_{34} + \sqrt{R_{34}^2 - R_3^2 (1 - \cos^2\theta_{34})}$$

$$R_1 = R_4 \cos\theta_{14} - \sqrt{R_{14}^2 - R_4^2 (1 - \cos^2\theta_{14})}$$

Set III

$$R_2 = R_1 \cos\theta_{12} + \sqrt{R_{12}^2 - R_1^2 (1 - \cos^2\theta_{12})}$$

$$R_4 = R_2 \cos\theta_{24} + \sqrt{R_{24}^2 - R_2^2 (1 - \cos^2\theta_{24})}$$

$$R_1 = R_4 \cos\theta_{14} - \sqrt{R_{14}^2 - R_4^2 (1 - \cos^2\theta_{14})}$$

The fourth source is present for two reasons. The first is to provide the sensor system with an option for choosing the best combination of three sources for solution of a triangle which yields the more accurate range results, or to select sources which fall within the sensor field of view at close ranges.

The second reason relates to the general case where the individual sources are not identifiable, either by signature

or by their relative position in the configuration pattern as viewed by the sensor. Under these circumstances the fourth source allows the development of three sets of equations in order that the computer can check for possible ambiguity in the solutions for range. Hence two sets of equations should be solved and agreement between solutions achieved to insure that the correct solutions have been attained.

The configuration described in Section 1.3 provides a means for the computer to identify all sources and avoid the need for computing and comparing results for more than one set of three sources to obtain unambiguous ranges to the sources.

One procedure for solution of the simultaneous equations is to let R_1 equal the maximum operational range for the device and solve for R_2, R_3, and/or R_4 as the case may be. The solution for R_1 is compared with the input value for R_1 and the difference taken. The input value of R_1 is then decreased by 50%, for example, and another computation made. Again the "R_1 in" is compared with the "R_1 out", the difference taken and the difference tested for polarity change. If no polarity change occurs, the "R_1 in" is again reduced to 50% of its last value and the procedure repeated until a polarity change in the difference occurs.

When the polarity change does occur, the last selected value for "R_1 in" is increased by 50% of its value and the polarity of the difference between "R_1 in" and "R_1 out" is tested. This procedure, increasing or decreasing "R_1 in" by 50% of each increment taken, is repeated until the difference between "R_1 in" and "R_1 out" is consistent with the desired error level.

Faster convergence to a solution for the ranges can be realized if interpolation or extrapolation techniques are employed should the real time consumption be undesirable.

Once the ranges have been obtained, the solution for the relative attitude between the two vehicles can be achieved. By definition, the following angles represent the rotation of the subject coordinates with respect to the reference coordinate system:

γ_1 - rotation about the x-axis

γ_2 - rotation about the displaced y-axis

γ_3 - rotation about the displaced z-axis

A transfer matrix, M, describing the relative attitude between sensor and source coordinate systems may be developed.

$$M = M_z \, M_y \, M_x$$

where

$$M_z = \begin{bmatrix} \cos\gamma_3 & \sin\gamma_3 & 0 \\ -\sin\gamma_3 & \cos\gamma_3 & 0 \\ 0 & 0 & 1 \end{bmatrix}$$

$$M_y = \begin{bmatrix} \cos\gamma_2 & 0 & -\sin\gamma_2 \\ 0 & 1 & 0 \\ \sin\gamma_2 & 0 & \cos\gamma_2 \end{bmatrix}$$

$$M_x = \begin{bmatrix} 1 & 0 & 0 \\ 0 & \cos\gamma_1 & \sin\gamma_1 \\ 0 & -\sin\gamma_1 & \cos\gamma_1 \end{bmatrix}$$

$$M = \begin{bmatrix} m_{11} & m_{12} & m_{13} \\ m_{21} & m_{22} & m_{23} \\ m_{31} & m_{32} & m_{33} \end{bmatrix}$$

where

$$m_{11} = \cos\gamma_2 \cos\gamma_3$$

$$m_{12} = \sin\gamma_1 \sin\gamma_2 \cos\gamma_3 + \cos\gamma_1 \sin\gamma_3$$

$$m_{13} = -\cos\gamma_1 \sin\gamma_2 \cos\gamma_3 + \sin\gamma_1 \sin\gamma_3$$

$$m_{21} = -\cos\gamma_2 \sin\gamma_3$$

$$m_{22} = -\sin\gamma_1 \sin\gamma_2 \sin\gamma_3 + \cos\gamma_1 \cos\gamma_3$$

$$m_{23} = \cos\gamma_1 \sin\gamma_2 \sin\gamma_3 + \sin\gamma_1 \cos\gamma_3$$

$$m_{31} = \sin\gamma_2$$

$$m_{32} = -\sin\gamma_1 \cos\gamma_2$$

$$m_{33} = \cos\gamma_1 \cos\gamma_2$$

The placement of the sources in subject coordinates is described by the vectors:

$\bar{R}_{12}$, $\bar{R}_{13}$, $\bar{R}_{14}$, $\bar{R}_{23}$, $\bar{R}_{24}$, and $\bar{R}_{34}$ as shown in Figure 2.

Let $\bar{R}_{1i}$ represent one of the vectors which exist between the subject coordinate system origin (source 1) and any other source on the subject.

$$\bar{R}^{R}_{1i} = M^{T}\bar{R}^{S}_{1i}$$

or

$$M\,\bar{R}^{R}_{1i} = \bar{R}^{S}_{1i}$$

where the superscript identifies the coordinate system in which the vector is resolved, and M^{T} is the transpose of M.

$$M \begin{bmatrix} | & | & | \\ \bar{R}^{R}_{12} & \bar{R}^{R}_{13} & \bar{R}^{R}_{14} \\ | & | & | \end{bmatrix} = \begin{bmatrix} | & | & | \\ \bar{R}^{S}_{12} & \bar{R}^{S}_{13} & R^{S}_{14} \\ | & | & | \end{bmatrix}$$

$$M = \begin{bmatrix} | & | & | \\ \bar{R}^{S}_{12} & \bar{R}^{S}_{13} & \bar{R}^{S}_{14} \\ | & | & | \end{bmatrix} \begin{bmatrix} | & | & | \\ \bar{R}^{R}_{12} & \bar{R}^{R}_{13} & \bar{R}^{R}_{14} \\ | & | & | \end{bmatrix}^{-1}$$

From Figure 1:

$$\bar{R}_{12} = \bar{R}_2 - \bar{R}_1,\ \bar{R}_{13} = \bar{R}_3 - \bar{R}_1,\ \text{and}\ \bar{R}_{14} = \bar{R}_4 - \bar{R}_1$$

In certain special cases such as the configuration shown in Figure 2, where $\bar{R}_{14}$ is shown in line with and parallel to $\bar{R}_{12}$, the cross products, $\bar{R}^{R}_{12} \times \bar{R}^{R}_{13}$ and $\bar{R}^{S}_{12} \times \bar{R}^{S}_{13}$, must be used in lieu of $\bar{R}^{R}_{14}$ and $\bar{R}^{S}_{14}$ respectively since the use of $\bar{R}_{14}$ would not allow completion of the matrix.

The solution for M above determines the angles γ_1, γ_2 and γ_3 which are solved as follows:

$$\sin\gamma_2 = m_{31}$$

$$\sin\gamma_3 = -\frac{m_{21}}{\cos\gamma_2} \quad ,$$

and

$$\sin\gamma_1 = -\frac{m_{32}}{\cos\gamma_2} \quad .$$

If any of the above angles are allowed to exceed 90° in magnitude, it is required to solve the following equations as necessary to avoid ambiguous answers.

$$\cos\gamma_1 = \frac{m_{33}}{\cos\gamma_2} \quad ,$$

$$\cos\gamma_2 = \frac{m_{21}}{\sin\gamma_3} \quad ,$$

and

$$\cos\gamma_3 = \frac{m_{11}}{\cos\gamma_2} \quad .$$

Finally, the position vector, $\bar{R}$, between the docking hatches or other location, such as an aim point, can be computed in the reference frame as follows:

$$\bar{R}^R = \bar{R}_1^R + M^T \bar{R}_{1D}^S - \bar{R}_{SD}^R$$

The information thus derived from this technique is now sufficient for a guidance system to control its own vehicle in any desired position or orientation with respect to the subject vehicle.

Another technique for solving this geometry is to employ the Law of Sines where again three sets of three equations are

developed allowing a solution for the ranges to be accomplished by methods similar to those previously described.

Iterative and other incrementing techniques can be employed to obtain solutions for the ranges, Euler angles, and relative position of the two vehicles or object.

Although the sensor coordinates have been used as the reference coordinates in this description, any convenient coordinate system can be selected as coordinates to accommodate specific applications.

2.0 Analysis Accomplished

2.1 Computer Simulation

Completion of the definition of the overall computer simulation program was accomplished. As presently configured in Figure 5, the simulation will evaluate the angle only sensor performance without the benefit of filtering or estimation techniques. It is further recognized that the random number generator is not a fully representative error model for the sensor. Boxes (2), (3), and (5) were completed and applicable flow charts are presented in Figures 6 through 10.

Consideration was given to the capability of simulating inputs from other type sensors, however this was not incorporated because of time and funding limitations.

In the interests of obtaining as much information about one sensor concept and the guidance laws selected, it was decided to proceed with the simulations as described.

Figure 6 shows that portion of the overall proposed simulation (Figure 5) which was programmed. Figures 7 through 10 support the information in Figure 6 by presenting in detail the logic necessary to accomplish the final results.

The purpose of the routine AZELUP (Figure 7) is to generate accurate solutions for the range, azimuth, and elevation to each source, given the range between the docking hatches, R_H and relative vehicle attitude. This operation thus computes the true values for the ranges which are used for evaluation purposes and the true values for azimuth and elevation angles which are fed to a summing network and to which are added instantaneous error signals from a random number generator.

MIT AUTOMATIC DOCKING SIMULATION WITH ANGLE ONLY SENSOR IMPLEMENTED

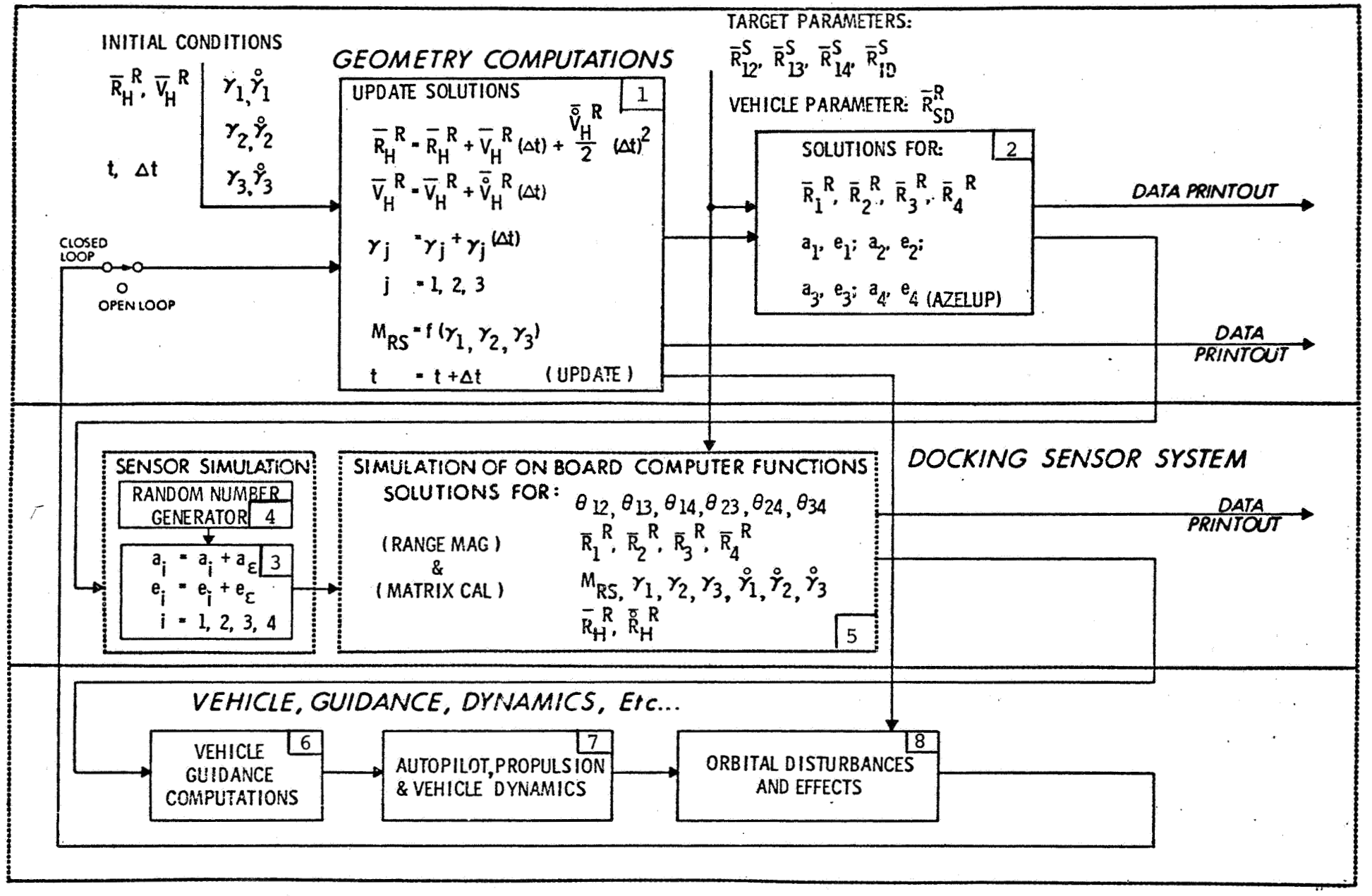

Figure 5

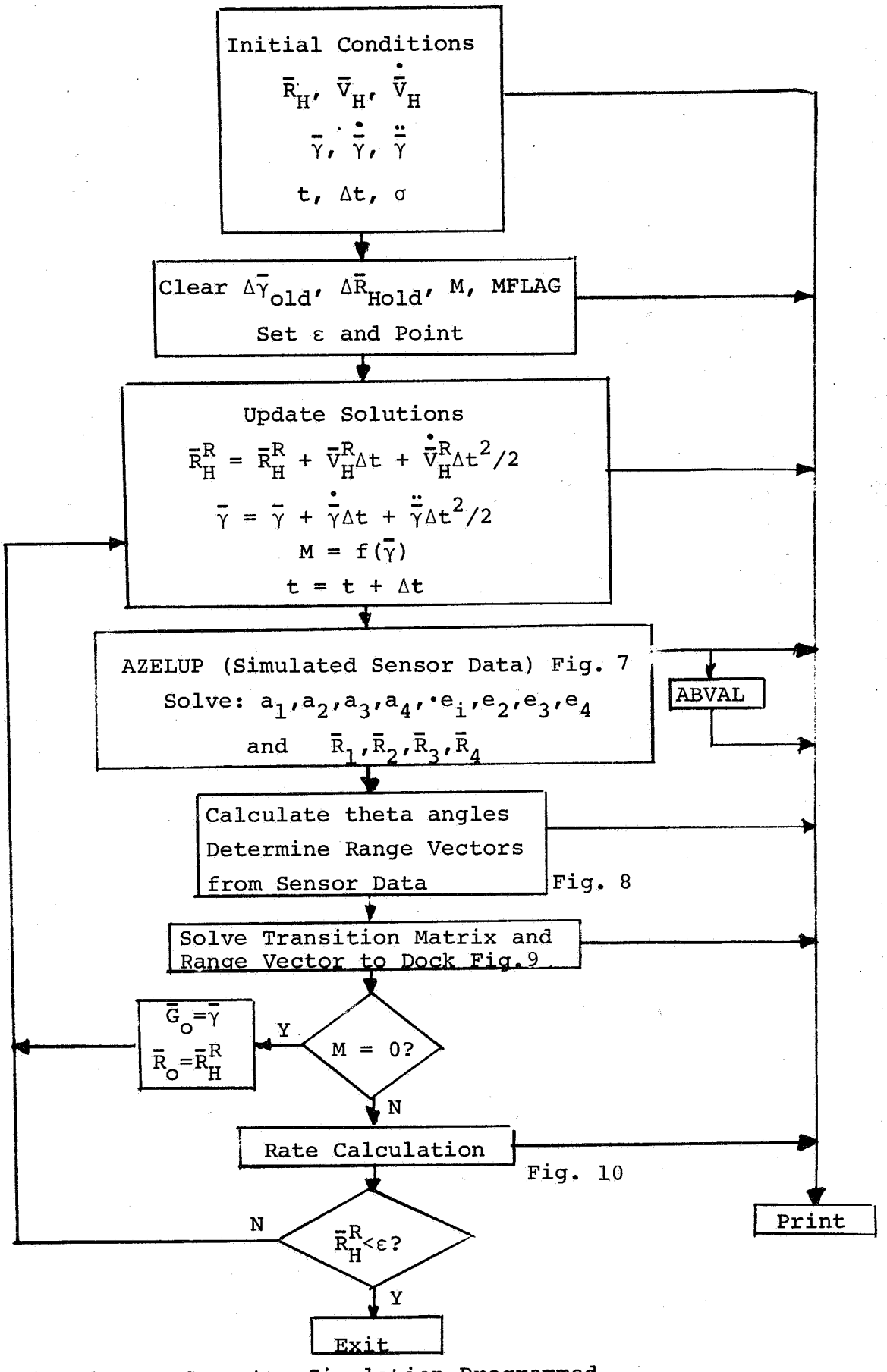

Fig. 6 MIT Computer Simulation Programmed

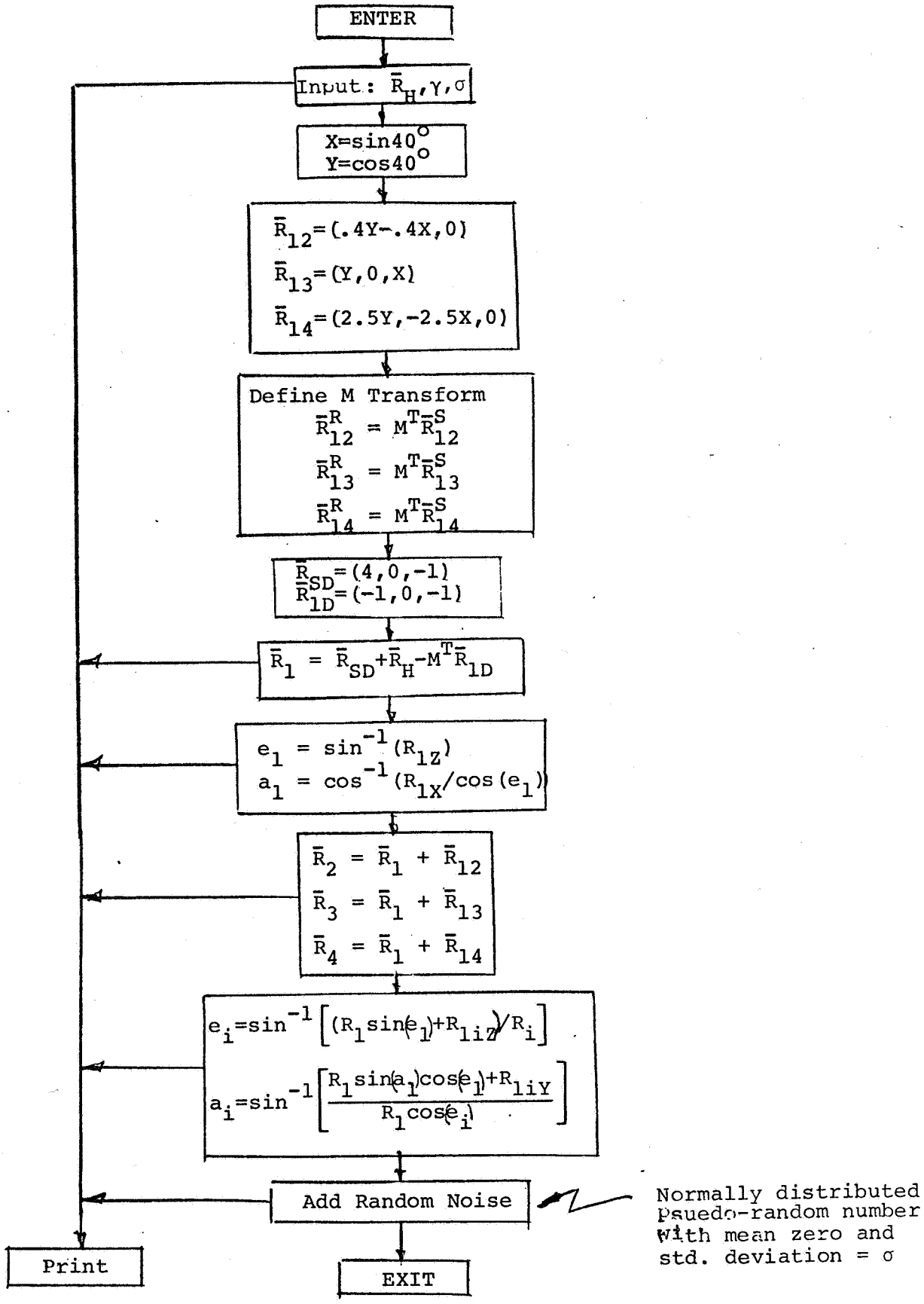

Fig. 7 AZELUP Subroutine

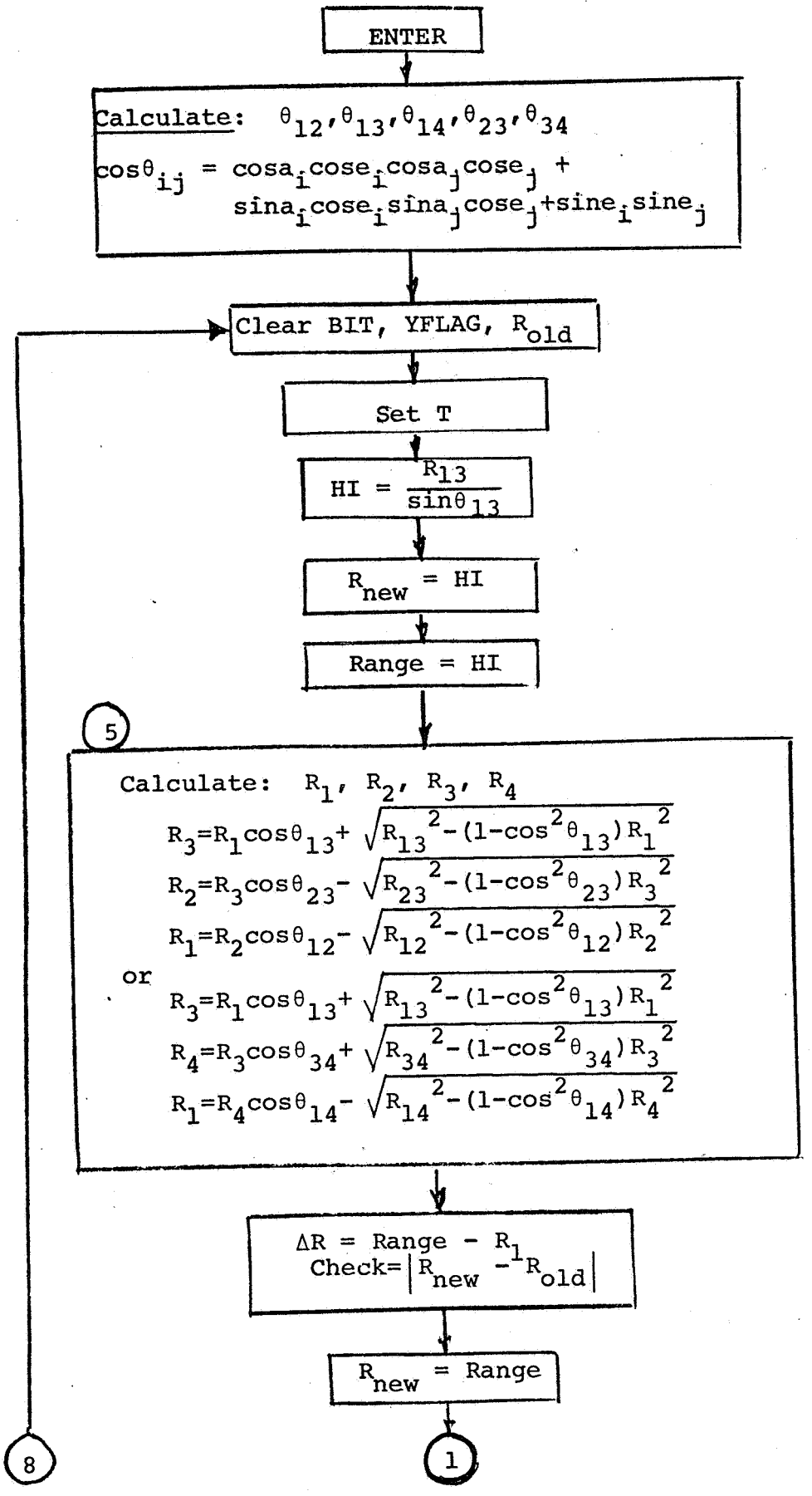

Fig. 8A Theta and Range Determination

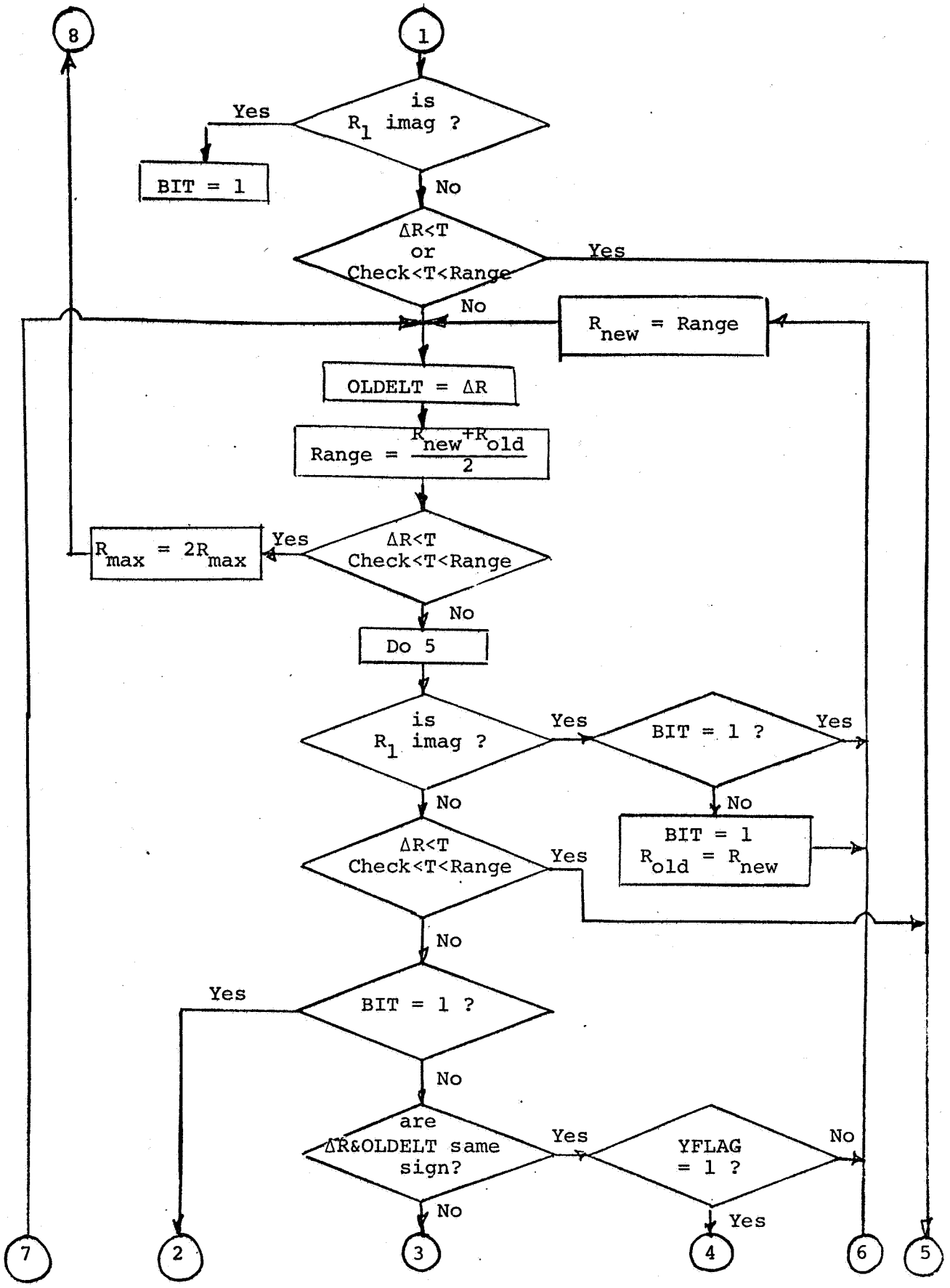

Fig. 8B Theta and Range Determination (Cont.)

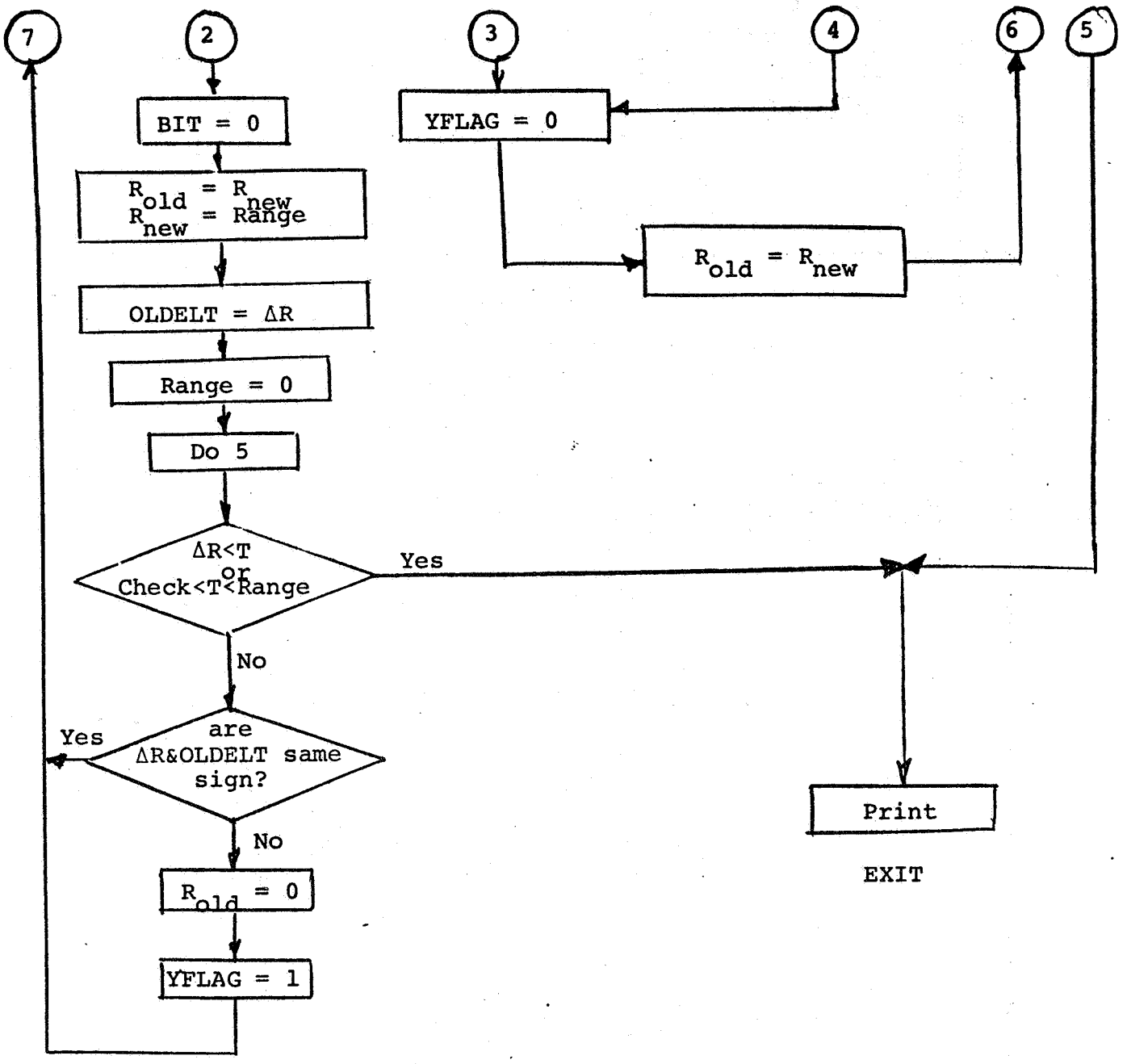

Fig. 8C Theta and Range Determination(Cont.)

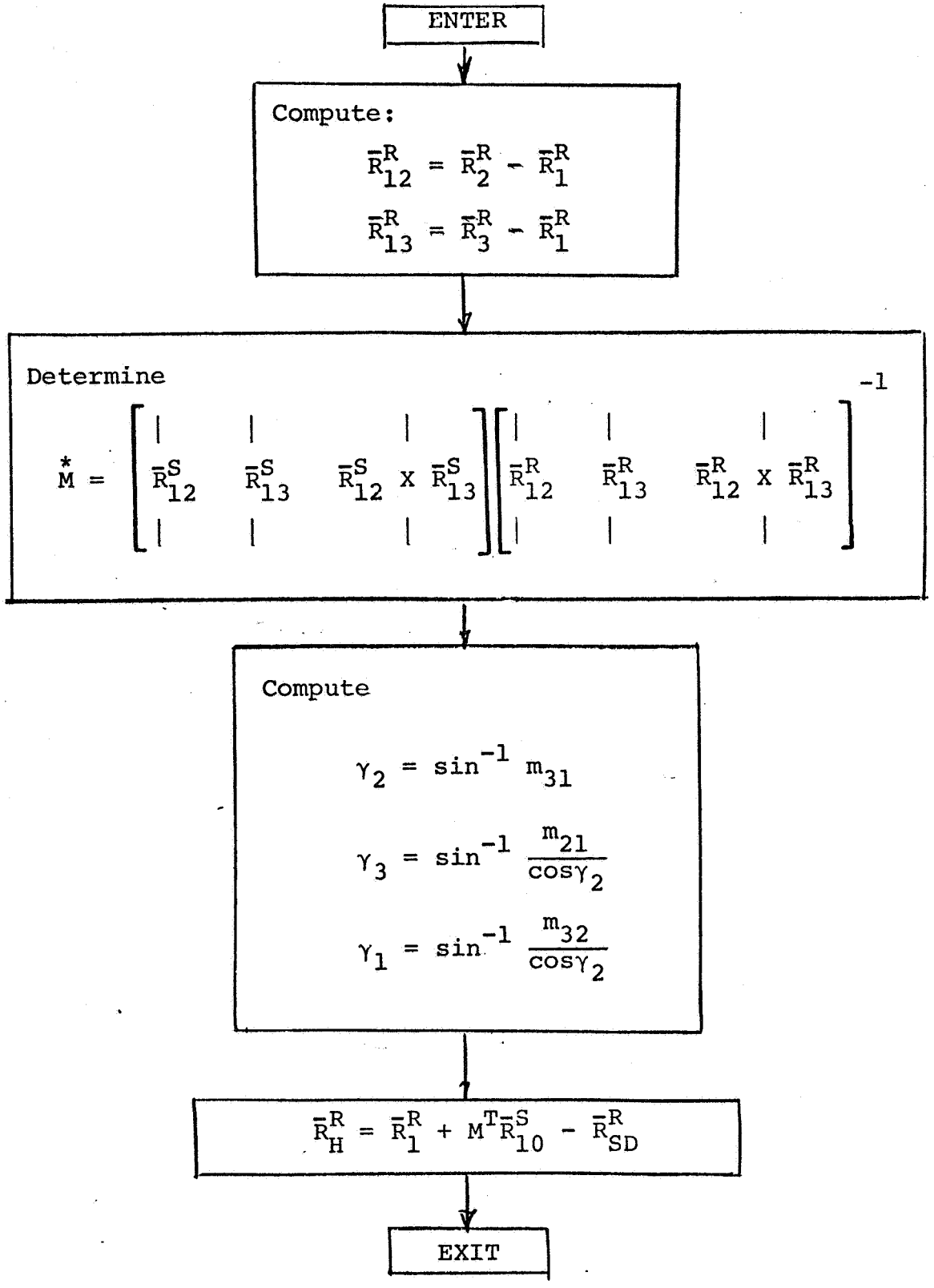

Fig. 9 Matrix and Docking Range Determination

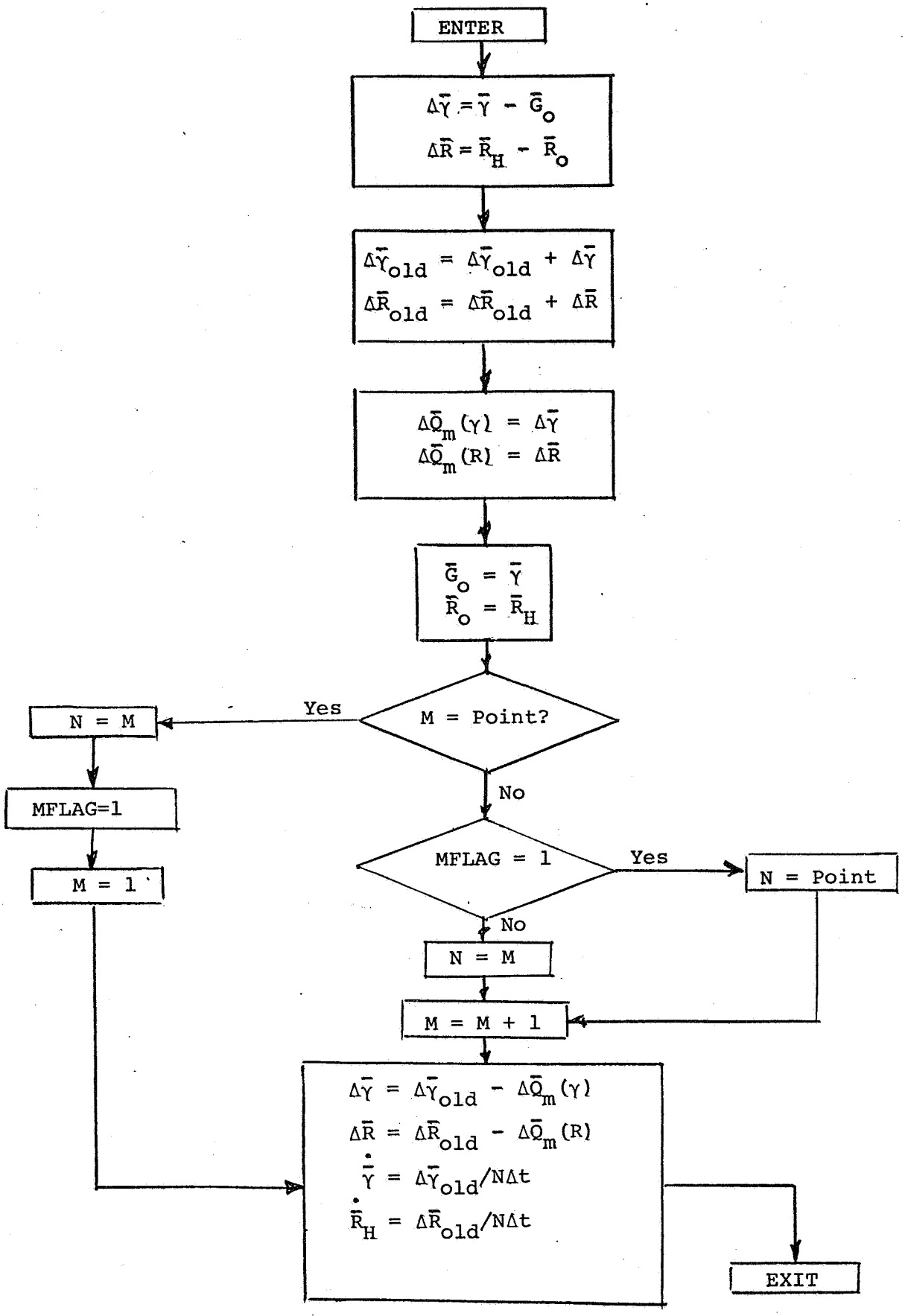

Fig. 10 Rate Calculations

This latter activity thus simulates the sensor accuracy characteristics. The portion of the simulation which computes the value of the angles between sources and the ranges to the sources and the portion which develops the Transformation Matrix, solves the Euler angles and computes the range $\bar{R}_H$, between docking hatches and the angle and range rates all have results dependent upon the errors introduced by the random number generator.

Several runs were made using the operating portion of the direct (unfiltered) simulation. These tests verified the functional feasibility of the computer programs designed to accept the raw sensor data, compute the ranges to the targets, and develop the relative position and attitude between vehicles. The sensor was initially located on the passive vehicle docking hatch axis 305 feet distant from source number one of the array shown in Fig. 2, i.e. R_1 = 305 feet. The initial closing rate was 10 feet per second, and at 40 feet distant reduced to 5 feet per second, at 9 feet to 1 foot per second, and at 8.9 feet to 0.1 foot per second.

Table 1 presents the results of a run made under the above conditions using target sources 1, 3, and 4. A single set of readings was made at each relative range sampled. The presentation shows the expected result of improved accuracy as the range decreases. The lateral position errors are considerably less than the track errors at long ranges. The track errors, however, improve much faster than the lateral errors as range decreases and at dock (when R_1 = 5 feet) all orthogonal errors are of the same order of magnitude. The velocity, angle, and angle rate errors are consistent with the position errors and show vast improvement as range decreases.

It should be remembered that the target array dimensions were not optimized for the geometry studied and that sensor

TABLE 1

Position, Velocity, Angle and Angle Rate Errors vs. Range
Derived From Computations Using Simulated Raw Sensor Single Measurement Data

RANGE	POSITION ERROR FEET			VELOCITY ERROR FEET/SEC			ANGLE ERROR DEGREES			ANGLE RATE ERROR DEGREES/SEC		
	X	Y	Z	$\dot{X}$	$\dot{Y}$	$\dot{Z}$	θ_x	θ_y	θ_z	$\dot{\theta}_x$	$\dot{\theta}_y$	$\dot{\theta}_z$
295	7.71	0.10	0.56	13.92	0.12	0.24	8.83	10.32	4.32	0.72	2.27	0.03
275	8.27	0.12	0.36	4.83	0.12	0.01	2.31	9.31	1.23	2.41	0.42	1.84
255	31.81	0.02	0.06	5.12	0.05	0.08	4.48	4.09	10.48	2.81	2.43	1.24
235	14.67	0.25	0.21	0.32	0.01	0.05	2.87	0.34	6.11	0.56	1.66	0.07
215	1.84	0.08	0.05	13.41	0.09	0.02	1.15	1.12	0.19	0.57	1.23	1.47
195	16.75	0.18	0.09	10.36	0.08	0.05	0.89	3.55	6.34	1.19	0.21	1.17
175	28.65	0.22	0.77	3.60	0.01	0.01	10.03	8.96	3.56	0.04	0.55	0.27
155	30.46	0.25	0.65	9.20	0.12	0.17	6.67	7.33	1.25	1.71	1.01	0.50
135	26.70	0.16	0.51	4.61	0.01	0.07	8.46	3.21	2.84	0.89	0.33	0.80
115	10.35	0.08	0.10	2.59	0.03	0.03	7.06	2.69	0.53	2.29	1.43	0.68
95	3.78	0.08	0.02	0.73	0.00	0.01	0.91	0.74	2.87	0.25	0.32	0.50
75	5.51	0.13	0.18	1.33	0.01	0.01	0.82	1.60	0.26	0.75	0.51	0.05
55	2.24	0.08	0.06	1.58	0.05	0.00	1.18	0.94	0.48	0.94	1.05	0.51
35	1.63	0.04	0.13	3.78	0.02	0.01	1.79	1.64	0.31	0.19	0.01	0.11
15	0.24	0.01	0.04	0.46	0.01	0.05	0.46	0.45	0.29	0.65	0.70	0.26
10	0.17	0.01	0.05	0.36	0.01	0.04	0.77	0.70	0.15	0.51	0.47	0.09
8	0.01	0.01	0.00	0.08	0.00	0.01	0.23	0.10	0.04	0.07	0.03	0.04
6.5	0.04	0.01	0.00	0.11	0.00	0.00	0.20	0.27	0.22	0.01	0.02	0.04
6.0	0.06	0.01	0.01	0.10	0.00	0.00	0.27	0.02	0.14	0.09	0.06	0.07
5.5	0.02	0.00	0.01	0.08	0.00	0.00	0.07	0.18	0.24	0.04	0.03	0.02
5.2	0.00	0.00	0.01	0.10	0.00	0.00	0.03	0.20	0.19	0.02	0.06	0.06

scale change was not implemented to compensate for the large dynamic range covered during the run. It is precisely these parameters that must be optimized for a given docking profile and geometry. Section 2.3 describes the improvement realizable using Kalman filtering which in addition to sensor/target parameter optimization makes the angle only sensor system appear feasible for SSV docking.

2.2 Guidance Law for Spacecraft Docking

2.2.1 General

There are two separate guidance phases involved with the docking operation. The first phase is the guiding of the sensor vehicle from a location near the edge of the operating cone at some large range to an aim point several hundred feet in front of the subject vehicle docking hatch on the docking axis. During this period, simultaneous control of both position and attitude of the sensor vehicle is desirable to insure that protrusions such as wings, arms, etc. from each vehicle do not interfere or collide, and to insure arrival at the aim point with the proper attitude. Figure 11 shows the desired docking profile for this phase.

The requirement for simultaneous control in translation and attitude and the establishment of an acceptable time both for arrival at an aim point and for the complete docking operation, make this guidance law somewhat unique and different from currently employed guidance laws. A very significant aspect of the law is the controlling of the vehicle attitude and attitude change in order to optimize convergence time with minimal expenditure of fuel. It is desirable to set up an initial rotational impulse about all three vehicle axes such

Figure 11

SAMPLE DOCKING TRAJECTORY

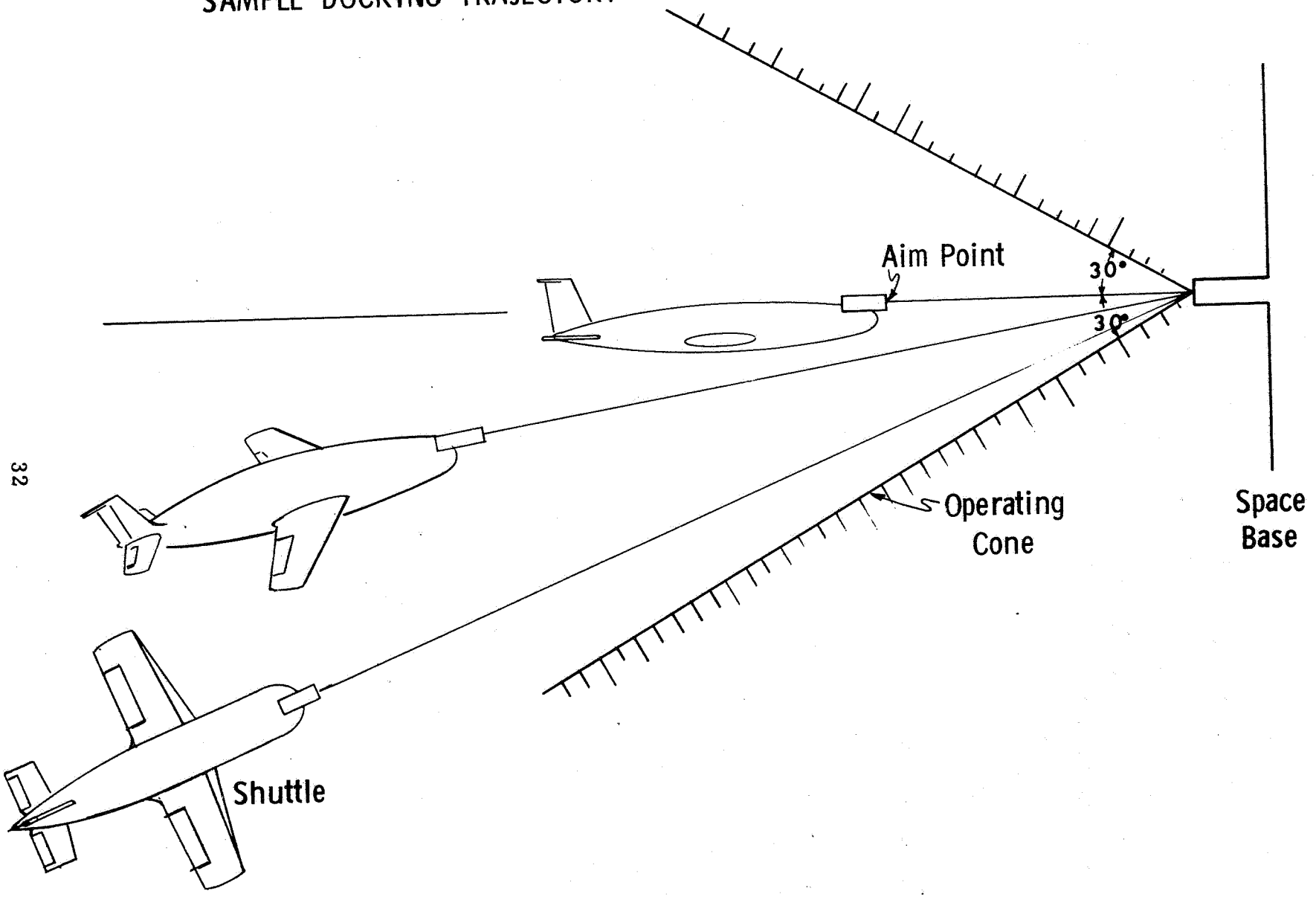

that upon arrival at an aim point a second set of impulses will reduce the rotational rates to zero with the vehicle attitude aligned for completion of the docking operation. An important parameter in docking guidance is the sensor vehicle angular momentum which, in the absence of external forces, remains constant as the vehicle rotates. The final equations for the guidance provide for the control of angular momentum rather than angle velocity.

The second phase, operating from the aim point to hard dock, also requires vehicle control in both position and attitude. However, the excursions in attitude and in position are expected to be small, requiring less correction energy than those of the pre-aim point phase. The range rate profile will call for the decreasing of approach velocity and corrections for small off-axis velocity build up as the sensor vehicle closes with the subject.

The guidance law should impose one additional restriction; the source array on the subject vehicle must be maintained within the field-of-view of the sensor at all times during the entire convergence operation for safety reasons. Computer runs have indicated that the sensor x-axis and the line-of-sight to the target array become misaligned during the simultaneous translation and rotation maneuver.

This study also considered a simplification of the guidance law. The most likely scheme was to initially roll the SSV such that its +z-axis would intersect the Space Station docking hatch axis line and then continue with rotation about the pitch axis only until an "Aim" point had been reached where another roll maneuver would place the SSV into proper orientation at this "Aim" point. The advantage that this technique

has is that angular velocities can be controlled directly rather than the need to control overall angular momentum. The principal disadvantages are that additional Δv is consumed to perform the two separate roll maneuvers, rotation about the axis of intermediate inertia (the y or pitch axis) is unstable, and the fact that all errors are not simultaneously reduced. This latter situation could create a misalignment condition just as docking occurred; however, since the errors should be small at that point, this may not be too serious.

2.2.2 Guidance Equations

2.2.2.1 Guidance Law Employing Simultaneous Translation and Rotation

The translational portion of the motion is reasonably easy to implement since the relative velocity and the linear momentum should be along the displacement vector. The rotational part of the motion is more difficult to analyze. An untorqued body rotates with constant angular momentum which (unless the three moments of inertia are equal) does not in general lie along the angular velocity. The parallelism of velocity and momentum applies to translational motion but not rotational.

The shuttle's three principal moments of inertia are unequal and its untorqued motion can be exactly described by elliptic functions. However the equations are somewhat involved and perhaps it is not necessary to use exact equations since there are errors associated with the sightings taken during the motion and corrective thrusting may occasionally be required. Two of the shuttle's moments J_y and

J_z are nearly equal and each is about ten times J_x. If J_z exactly equaled J_y, then the rotational motion would be described by

$$\dot{\theta}_1 = H/J_y \quad \text{(constant)} \tag{1}$$

$$\theta_2 = \text{constant} \tag{2}$$

$$\dot{\theta}_3 = \dot{\theta}_1 \left(\frac{J_y}{J_x} - 1 \right) \cos\theta_2 \quad \text{(constant)} \tag{3}$$

where H is the angular momentum magnitude and θ_1, θ_2, and θ_3 are a set of angles relating the shuttle axes and a set of inertial axes. It is proposed to use this description of the rotation as a reference and then, if increased accuracy is desired, to perturb these equations using the quantity $\frac{J_z - J_y}{J_x}$ as a parameter.

ROTATION OF A SYMMETRIC BODY ($J_y = J_z$)

The preceding equations are derived as follows. Let H denote the angular momentum of the shuttle about its center of mass. Then $\bar{H} = J\bar{\omega}$ where J is the shuttle's moment-of-inertia tensor and $\bar{\omega}$ is the shuttle's inertial angular velocity. The dynamical law of rotation states that the inertial derivative of $\bar{H}$ is the sum of the torques $\bar{T}$ acting on the body, $\dot{\bar{H}} = \bar{T}$ or

$$J\dot{\bar{\omega}} + \bar{\omega} \times J\bar{\omega} = \bar{T}$$

Here the first term is the derivative of $\bar{H}$ with respect to shuttle axes and the second term is the Coriolis correction. Variations of J with respect to the shuttle are ignored. The components of this equation along principal axes are the Euler equations

$$J_x\dot{\omega}_x + (J_z - J_y)\omega_y\omega_z = T_x$$

$$J_y\dot{\omega}_y + (J_x - J_z)\omega_z\omega_x = T_y$$

$$J_z\dot{\omega}_z + (J_y - J_x)\omega_x\omega_y = T_z \qquad (4)$$

If Torques are absent and if J_z equals J_y,

$$J_x\dot{\omega}_x = 0$$

$$J_y\dot{\omega}_y - (J_y - J_x)\omega_x\omega_z = 0$$

$$J_y\dot{\omega}_z + (J_y - J_x)\omega_x\omega_y = 0 \qquad (4a)$$

Then ω_x remains constant at its initial value ω_{x_0} and

$$\dot{\omega}_y - C\omega_z = 0$$

$$\dot{\omega}_z + C\omega_y = 0 \qquad (4b)$$

where

$$C = (1 - \frac{J_x}{J_y})\omega_x$$

$$\omega_x = \omega_{x_0} \qquad (4c)$$

The solution of the differential equation is

$$\omega_y = \omega_{y_0}\ \text{cosCt} + \omega_{z_0}\ \text{sinCt}$$

$$\omega_z = -\omega_{y_0}\ \text{sinCt} + \omega_{z_0}\ \text{cosCt} \qquad (4d)$$

When the torque is zero, the shuttle's angular momentum is constant. Define an inertial axis system $x_I y_I z_I$ with x_I along the constant $\bar{H}$ and y_I and z_I perpendicular to $\bar{H}$ (the

latter two axes need not be more explicitly defined here). Let θ_1, θ_2, and θ_3 be the set of Euler angles relating the shuttle axes xyz to $x_I y_I z_I$ where θ_1 is measured about $\bar{H}$, θ_2 is the angle between this vector and the shuttle's x-axis, and θ_3 is measured about the latter axis. With

θ_1 about x_I

θ_2 about intermediate y

θ_3 about (shuttle's) x

The matrix P of direction cosines from $x_I y_I z_I$ to xyz is obtained as the product

$$P = \begin{bmatrix} 1 & 0 & 0 \\ 0 & \cos\theta_3 & \sin\theta_3 \\ 0 & -\sin\theta_3 & \cos\theta_3 \end{bmatrix} \begin{bmatrix} \cos\theta_2 & 0 & -\sin\theta_2 \\ 0 & 1 & 0 \\ \sin\theta_2 & 0 & \cos\theta_2 \end{bmatrix} \begin{bmatrix} 1 & 0 & 0 \\ 0 & \cos\theta_1 & \sin\theta_1 \\ 0 & -\sin\theta_1 & \cos\theta_1 \end{bmatrix} \tag{4e}$$

$$P = \begin{bmatrix} \cos\theta_2 & 0 & -\sin\theta_2 \\ \sin\theta_2\sin\theta_3 & \cos\theta_3 & \cos\theta_2\sin\theta_3 \\ \sin\theta_2\cos\theta_3 & -\sin\theta_3 & \cos\theta_2\cos\theta_3 \end{bmatrix} \begin{bmatrix} 1 & 0 & 0 \\ 0 & \cos\theta_1 & \sin\theta_1 \\ 0 & -\sin\theta_1 & \cos\theta_1 \end{bmatrix} \tag{5}$$

or

$$P = \begin{bmatrix} \cos\theta_2 & \sin\theta_1\sin\theta_2 & -\cos\theta_1\sin\theta_2 \\ \sin\theta_2\sin\theta_3 & & \\ \sin\theta_2\cos\theta_3 & & \end{bmatrix}$$

where the remaining four entries need not be calculated. The

inertial angular velocity $\bar{\omega}$ of the shuttle is the vectorial sum of the Euler angle rates about their respective axes. Thus

$$\bar{\omega} = \dot{\theta}_3\bar{i} + \dot{\theta}_2(\bar{j}\cos\theta_3 - \bar{k}\sin\theta_3)$$

$$+ \dot{\theta}_1(\bar{i}\cos\theta_2 + \bar{j}\sin\theta_2\sin\theta_3 + \bar{k}\sin\theta_2\cos\theta_3)$$

where the components of the θ_1 and θ_2 axes are given by the first and second solumns of the first matrix in (5). The components of $\bar{\omega}$ are

$$\omega_x = \dot{\theta}_1\cos\theta_2 + \dot{\theta}_3 \tag{6}$$

$$\omega_y = \dot{\theta}_1\sin\theta_2\sin\theta_3 + \dot{\theta}_2\cos\theta_3 \tag{7}$$

$$\omega_z = \dot{\theta}_1\sin\theta_2\cos\theta_3 - \dot{\theta}_2\sin\theta_3 \tag{8}$$

The angular momentum $\bar{H}$ is

$$\bar{H} = H\bar{i}_I$$

or

$$\bar{H} = H(\bar{i}\cos\theta_2 + \bar{j}\sin\theta_2\sin\theta_3 + \bar{k}\sin\theta_2\cos\theta_3) \quad .$$

Thus

$$H_x = J_x\omega_x = H\cos\theta_2$$

$$H_y = J_y\omega_y = H\sin\theta_2\sin\theta_3 \tag{9}$$

$$H_z = J_z\omega_z = H\sin\theta_2\cos\theta_3$$

Since ω_x is constant, it follows that θ_2 is constant. It is next shown that $\dot{\theta}_1$ and $\dot{\theta}_3$ are constant. Let K denote the dot product of $\bar{\omega}$ and $\bar{H}$. (This quantity is twice the kinetic energy of rotation.)

$$K = \bar{\omega} \cdot \bar{H} = J_x\omega_x^2 + J_y\omega_y^2 + J_z\omega_z^2 \qquad (10)$$

In terms of row and column vectors,

$$K = \bar{\omega}^T J\bar{\omega} \qquad *$$

Differentiating,

$$\dot{K} = \dot{\bar{\omega}}^T J\bar{\omega} + \bar{\omega}^T J\dot{\bar{\omega}} \qquad *$$

or

$$\dot{K} = (\bar{\omega}^T J^T\dot{\bar{\omega}})^T + \bar{\omega}^T J\dot{\bar{\omega}} \qquad *$$

Since J is symmetric

$$\dot{K} = 2\bar{\omega}^T J\dot{\bar{\omega}} = 2\bar{\omega} \cdot J\dot{\bar{\omega}} \qquad *$$

Adding a quantity which is identically zero gives

$$\dot{K} = 2\bar{\omega} \cdot (J\dot{\bar{\omega}} + \bar{\omega} \times J\bar{\omega})$$

But the term in the parentheses is the torque which is assumed to be zero. Thus

$$\dot{K} = 2\bar{\omega} \cdot \bar{T} = 0$$

and K is constant. Substitution of (9) into (10) gives K in terms of Euler angles,

$$K = J_x\omega_x^2 + \frac{H^2}{J_y}\sin^2\theta_2 \sin^2\theta_3 + \frac{H^2}{J_z}\sin^2\theta_2 \cos^2\theta_3$$

and since J_z equals J_y,

$$K = J_x\omega_x^2 + \frac{H^2}{J_y}\sin^2\theta_2 \qquad (11)$$

This result is used in a later equation. Multiplying (7) by

---

*"T" is used here to denote the transpose of a matrix as differentiated from torque in equation (4) preceding, and otherwise explained.

$\sin\theta_2$, (8) by $\cos\theta_3$, and adding gives

$$\omega_y \sin\theta_3 + \omega_z \cos\theta_3 = \dot{\theta}_1 \sin\theta_2$$

Multiplying both sides of this equation by $H\sin\theta_2$,

$$\omega_y H\sin\theta_2 \sin\theta_3 + \omega_z H\sin\theta_2 \cos\theta_3 = \dot{\theta}_1 H\sin^2\theta_2$$

and substituting from (9),

$$J_y\omega_y^2 + J_z\omega_z^2 = \dot{\theta}_1 H\sin^2\theta_2$$

or, from (10),

$$K - J_x\omega_x^2 = \dot{\theta}_1 H\sin^2\theta_2$$

and from (11),

$$\frac{H^2}{J_y}\sin^2\theta_2 = \dot{\theta}_1 H\sin^2\theta_2$$

so that

$$\dot{\theta}_1 = \frac{H}{J_y} \tag{12}$$

which is constant. It follows (6) that

$$\dot{\theta}_3 = \omega_x - \dot{\theta}_1 \cos\theta_2$$

and $\dot{\theta}_3$ is constant. Another formula for $\dot{\theta}_3$ is derived below. From the first of (9),

$$\dot{\theta}_3 = \frac{H}{J_x}\cos\theta_2 - \frac{H}{J_y}\cos\theta_2$$

or

$$\dot{\theta}_3 = \frac{H}{J_y}\left(\frac{J_y}{J_x} - 1\right)\cos\theta_2 \tag{12a}$$

and

$$\dot{\theta}_3 = \dot{\theta}_1\left(\frac{J_y}{J_x} - 1\right)\cos\theta_2 \qquad (13)$$

The result that the angle θ_2 and the angular rates $\dot{\theta}_1$ and $\dot{\theta}_2$ are constant for a body with two equal moments of inertia (J_y and J_z) in the absence of torques gives rise to the description that the x-axis rotates at constant angular rate ($\dot{\theta}_1$) about and remains at a fixed angle (θ_2) from $\bar{H}$ (thereby tracing out a cone) while the body is rotating at a fixed rate ($\dot{\theta}_3$) about its x-axis.

DETERMINATION OF THE ANGULAR MOMENTUM

The preceding section shows how the continuing rotation of an untorqued symmetric body may be obtained when its initial orientation and angular momentum are given. For the present problem, the initial and final orientations are given and it is necessary to find the angular momentum vector required for achieving the final orientation.

If the initial values of θ_1 and θ_3 are defined to be zero, the final values θ_1^* and θ_3^* are obtained, by integrating (12) and (13), as

$$\theta_1^* = \frac{Ht^*}{J_y}$$

$$\theta_3^* = \theta_1^*\left(\frac{J_y}{J_x} - 1\right)\cos\theta_2 \qquad (14)$$

where t^* is the time of flight. Let α denote the angle between the initial and final x-axes and ϕ be measured about the final x-axis. These angles constitute a sequence of two rotations

taking the shuttle from its initial to its final orientation. Let β be the angle between the angular momentum vector and the plane containing the initial and final x-axes. Geometrical considerations show that

$$\cos\frac{\theta_1^*}{2} = \cos\frac{\theta_3^* - \phi}{2}\cos\frac{\alpha}{2} \tag{15}$$

$$\sin\frac{\theta_1^*}{2}\cos\quad = -\sin\frac{\theta_3^* - \phi}{2} \tag{16}$$

$$\sin\frac{\theta_1^*}{2}\sin\quad = \cos\frac{\theta_3^* - \phi}{2}\sin\frac{\alpha}{2} \tag{17}$$

$$\cos\theta_2 = \cos\frac{\alpha}{2}\cos\beta \tag{18}$$

The preceding four equations along with (14) provide a solution for angles θ_1^*, θ_2^*, θ_3^*, and β and then H is given by

$$H = \frac{J_y\theta_1^*}{t^*}$$

It should be noted that (15), (16), and (17) constitute a dependent set of equations because the sum of the squares of their left-hand sides is one. These equations are derived below. Let $\bar{i}$ denote the initial x-axis and $\bar{i}'$ denote the final x-axis of the shuttle. Let

$$\bar{k}' = \text{unit}(\bar{i} \times \bar{i}')$$

$$\bar{j}' = \bar{k}' \times \bar{i}'$$

The angles α, β, and θ_2 are illustrated in figure 12. The vector $\bar{i}'$ is obtained by rotating $\bar{i}$ about the unit angular momentum $\bar{i}_I$ through the angle θ_1^*. The equation of this rotation is

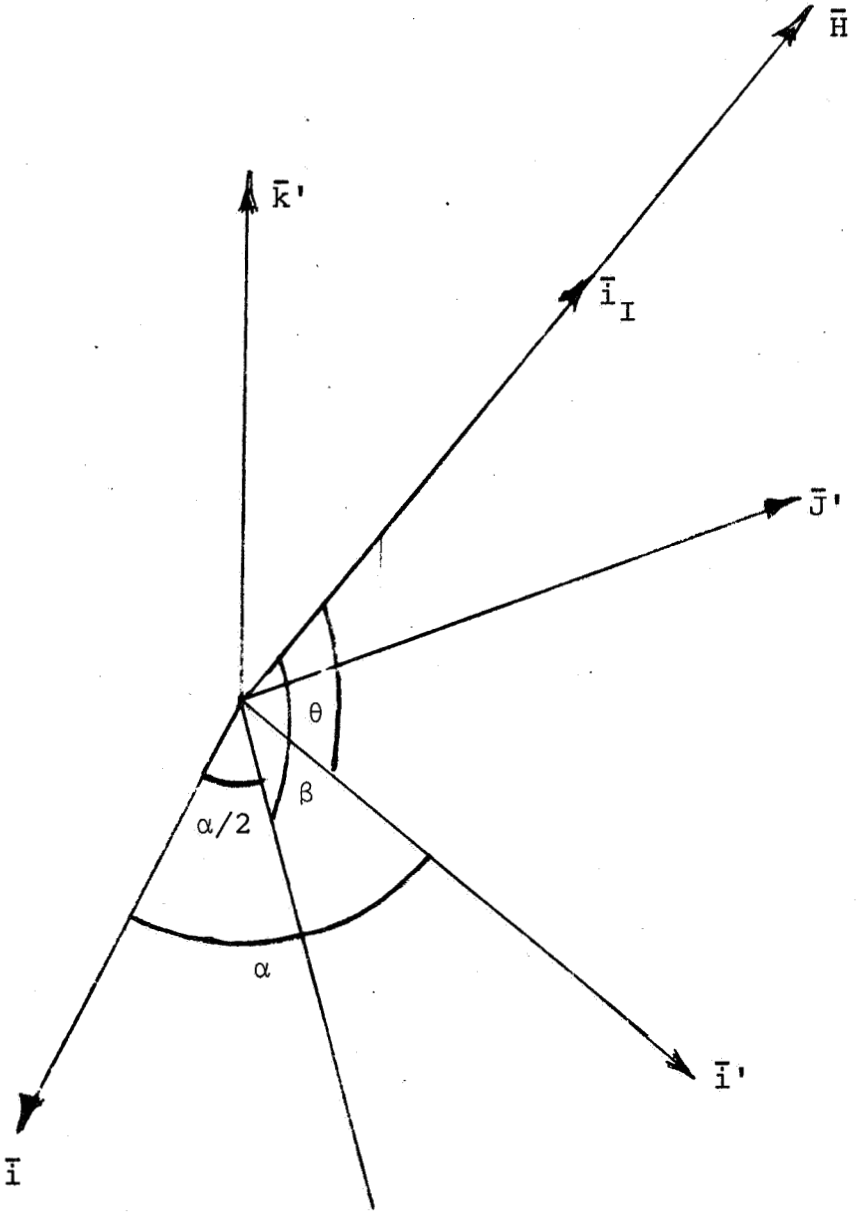

Figure 12. Angular Momentum Geometry.

$$\bar{i}' = \bar{i} + \bar{i}_I \times \bar{i}\sin\theta_1^* + \bar{i}_I \times (\bar{i}_I \times \bar{i})(1 - \cos\theta_1^*) \qquad (19)$$

Dotting this equation with $\bar{i}_I$ gives

$$\bar{i}_I \cdot \bar{i}' = \bar{i}_I \cdot \bar{i}$$

or

$$\bar{i}_I \cdot (\bar{i}' - \bar{i}) = 0$$

Dotting the difference $\bar{i}' - \bar{i}$ with the sum $\bar{i}' + \bar{i}$ gives

$$(\bar{i}' + \bar{i}) \cdot (\bar{i}' - \bar{i}) = \bar{i}' \cdot \bar{i}' - \bar{i} \cdot \bar{i} = 0$$

Finally

$$\bar{k}' \cdot (\bar{i}' - \bar{i}) = 0$$

Because these three dot products are zero,

$\bar{k}'$ is perpendicular to $\bar{i}' - \bar{i}$

$\bar{i}^* + \bar{i}'$ is perpendicular to $\bar{i}' - \bar{i}$

$\bar{i}_I$ is perpendicular to $\bar{i}' - \bar{i}$

and $\bar{i}_I$ lies in the plane of $\bar{k}'$ and $\bar{i}' + \bar{i}$. But $\bar{i}' + \bar{i}$ lies along the angle bisector of $\bar{i}'$ and $\bar{i}$. Therefore:

$$\bar{i}_I = \bar{i}'\cos\tfrac{\alpha}{2}\cos\beta - \bar{j}'\sin\tfrac{\alpha}{2}\cos\beta + \bar{k}'\sin\beta \qquad (20)$$

There are defined two sequences of rotations taking the shuttle from its initial to its final orientation. The first one is angle α about $\bar{k}'$ followed by angle ϕ about $\bar{i}'$ where these angles are specified by the two orientations. The second sequence is angle θ_1^* about $\bar{i}_I$ followed by θ_3^* about $\bar{i}'$. The latter two angles along with β, the elevation angle of $\bar{i}_I$ with respect to the plane of $\bar{i}$ and $\bar{i}'$, are to be determined.

The rotation between the two orientations is given by the quaternion product $p_\phi p_\alpha$ where

$$p_\phi = \cos\frac{\phi}{2} + \bar{i}'\sin\frac{\phi}{2}$$

$$p_\alpha = \cos\frac{\alpha}{2} + \bar{k}'\sin\frac{\alpha}{2}$$

The rotation is also given by the product $p_3 p_1$ where

$$p_3 = \cos\frac{\theta_3^*}{2} + \bar{i}'\sin\frac{\theta_3^*}{2}$$

$$p_1 = \cos\frac{\theta_1^*}{2} + \bar{i}_I\sin\frac{\theta_1^*}{2}$$

Thus

$$p_3 p_1 = p_\phi p_\alpha$$

or

$$p_1 = p_3^{-1} p_\phi p_\alpha$$

This expands into

$$p_1 = (\cos\frac{\theta_3^*}{2} - \bar{i}'\sin\frac{\theta_3^*}{2})(\cos\frac{\phi}{2} + \bar{i}'\sin\frac{\phi}{2})\,p_\alpha$$

or

$$p_1 = (\cos\frac{\theta_3^* - \phi}{2} - \bar{i}'\sin\frac{\theta_3^* - \phi}{2})(\cos\frac{\alpha}{2} + \bar{k}'\sin\frac{\alpha}{2})$$

so that

$$\cos\frac{\theta_1^*}{2} + \bar{i}_I \sin\frac{\theta_1^*}{2} = \cos\frac{\theta_3^* - \phi}{2}\cos\frac{\alpha}{2} - \bar{i}'\sin\frac{\theta_3^* - \phi}{2}\cos\frac{\alpha}{2}$$

$$+ \bar{j}'\sin\frac{\theta_3^* - \phi}{2}\sin\frac{\alpha}{2} + \bar{k}'\cos\frac{\theta_3^* - \phi}{2}\sin\frac{\alpha}{2}$$

Equating scalar and vector parts of this equation and using (20) gives

$$\cos\frac{\theta_1^*}{2} = \cos\frac{\theta_3^* - \phi}{2}\cos\frac{\alpha}{2}$$

$$\sin\frac{\theta_1^*}{2}\cos\frac{\alpha}{2}\cos\beta = -\sin\frac{\theta_3^* - \phi}{2}\cos\frac{\alpha}{2}$$

$$\sin\frac{\theta_1^*}{2}\sin\frac{\alpha}{2}\cos\beta = -\sin\frac{\theta_3^* - \phi}{2}\sin\frac{\alpha}{2}$$

$$\sin\frac{\theta_1^*}{2}\sin\beta = \cos\frac{\theta_3^* - \phi}{2}\sin\frac{\alpha}{2}$$

The middle two of these equations are equivalent to

$$\sin\frac{\theta_1^*}{2}\cos\beta = -\sin\frac{\theta_3^* - \phi}{2}$$

and (15) through (17) are verified. Since θ_2 is the angle between $\bar{i}'$ and $\bar{i}_I$, $\cos\theta_2$ is the dot product of $\bar{i}'$ and $\bar{i}_I$, and (18) is produced by dotting (20) with $\bar{i}'$.

NUMERICAL SOLUTION OF THE EQUATIONS

It is impossible to solve (14) through (18) analytically, so a numerical technique was devised. Division of (16) by (17) and (17) by (15) gives

$$\tan\frac{\theta_3^* - \phi}{2} = -\sin\frac{\alpha}{2}\cot\beta \tag{21}$$

$$\tan\frac{\theta_1^*}{2} = \tan\frac{\alpha}{2}\csc\beta \tag{22}$$

and substitution of (18) into (14) yields

$$\theta_3^* = \theta_1^*\left(\frac{J_y}{J_x} - 1\right)\cos\frac{\alpha}{2}\cos\beta \tag{23}$$

For a given α and ϕ, β is allowed to vary in the range $0 < \beta < 180^o$ until the solution for θ_1^* and θ_3^* from (22) and (21) satisfies (23).

This range for β is chosen so that $\alpha \leq \theta_1^* \leq 180^o$, that is, the shuttle's x-axis moves from its initial to it final orientation in the smaller of the two angles about the cone. This is proved as follows. The inverse of (19) is

$$\bar{i} = \bar{i}' - \bar{i}_I \times \bar{i}'\sin\theta_1^* + \bar{i}_I \times (\bar{i}_I \times \bar{i}')(1 - \cos\theta_1^*)$$

(which describes a rotation of $\bar{i}'$ about $-\bar{i}_I$ through the angle θ_1^*) or

$$\bar{i} = \bar{i}' - \bar{i}_I \times \bar{i}'\sin\theta_1^* + \left[(\bar{i}_I \cdot \bar{i}')\bar{i}_I - \bar{i}'\right](1 - \cos\theta_1)$$

Dotting this equation with $\bar{k}'$ gives

$$0 = \bar{i}_I \times \bar{i}' \cdot \bar{k}'\sin\theta_1^* + (\bar{i}_I \cdot \bar{i}')(\bar{i}_I \cdot \bar{k}')(1 - \cos\theta_1^*)$$

or

$$-\bar{i}_I \cdot \bar{j}'\sin\theta_1^* = (\bar{i}_I \cdot \bar{i}')(\bar{i}_I \cdot \bar{k}')(1 - \cos\theta_1^*)$$

Evaluating the dot products from (20) yields

$$\sin\frac{\alpha}{2}\cos\beta\sin\theta_1^* = \cos\frac{\alpha}{2}\cos\beta\sin\beta(1 - \cos\theta_1^*)$$

or

$$\sin\beta = \frac{\sin\theta_1^*}{1 - \cos\theta_1^*}\tan\frac{\alpha}{2}$$

so that

$$\sin\beta = \cot\frac{\theta_1^*}{2}\tan\frac{\alpha}{2} > 0$$

A computer program was written to check the existence of solutions of the equation. This program was run for α equal to 30° and ϕ taking on values at 10° steps in the range

$$-170^\circ \leq \phi \leq 170^\circ$$

For each case there is at least one, usually two, and occasionally three solutions for the angular momentum. It is assumed that similar results occur for a shuttle with unequal moments of inertia, but this should be checked.

The display of lights on the space station should remain within the field of view of the sensor on the shuttle during the latter's rotation and translation. The program was expanded to test this aspect of the motion. An initial range of 1000 feet and final ranges of 300 feet, 500 feet, and 866 feet were chosen for the aim point.

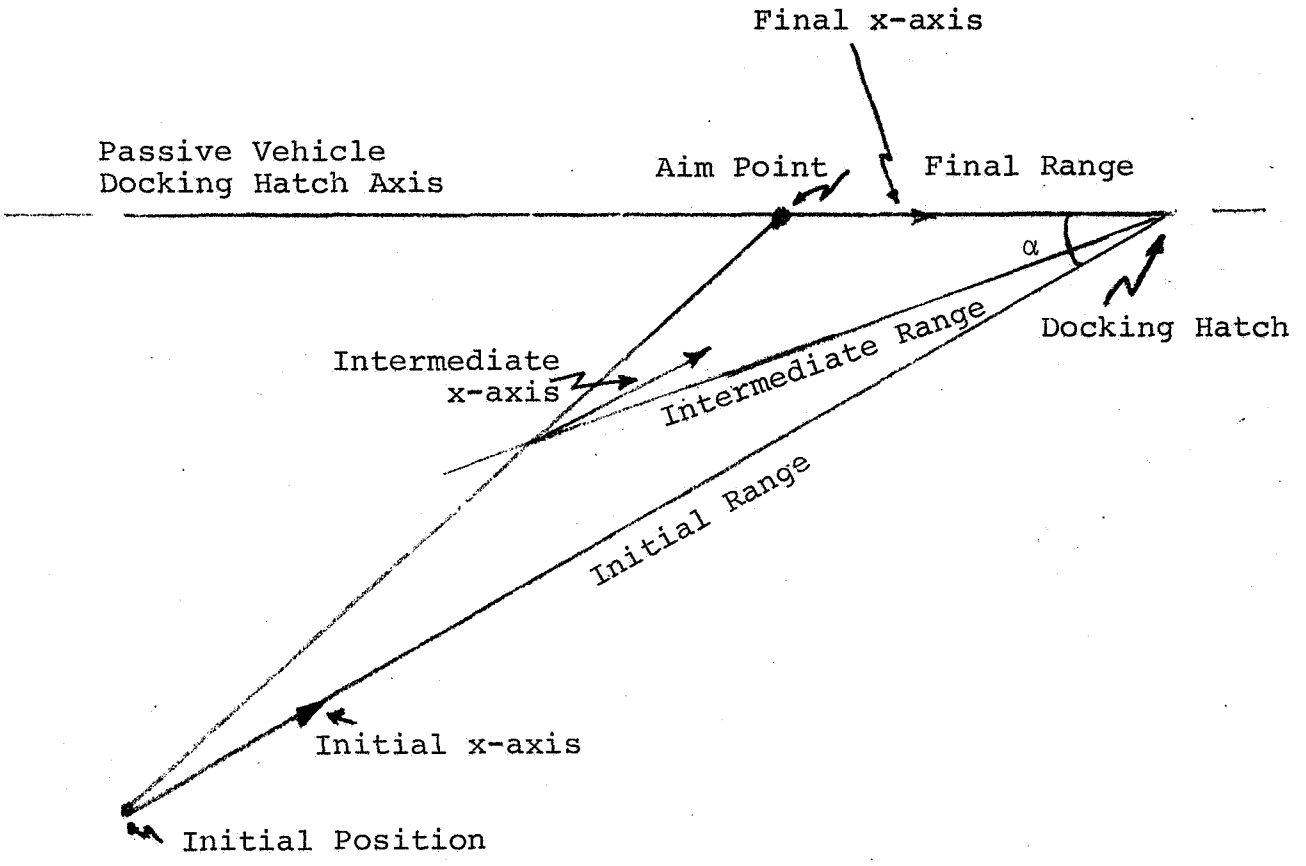

Figure 13. Conversion Geometry to Aim Point.

These runs indicate that the magnitude of maximum misalignment during coast is dependent upon the location of the aim point relative to the initial relative position of the shuttle. For example, if the shuttle is located at the edge of the $\pm 30^{o}$ cone surrounding the docking hatch axis of the passive vehicle and is 1000 feet distant, the deviation between the LOS and the sensor axis will become as high as 9 degrees during the simultaneous translation and rotational maneuver when the aim point

is located 300 feet in front of the passive vehicle docking hatch. When the aim point is roughly at the same range as the shuttle from the passive docking hatch the maximum deviation can be held to less than 3 degrees.

APPROXIMATE ROTATION OF AN ALMOST SYMMETRIC BODY ($J_y \simeq J_z$)

A method of determining the rotation of a body with two nearly equal moments of inertia is presented in this section. It consists of a first-order perturbation of the angular velocity equations for a symmetric body followed by the change in rotation caused by a perturbed angular velocity as described in the preceding section.

The perturbed equations corresponding to (4) preceding are (in the absence of torques)

$$J_x(\dot{\omega}_x + \Delta\dot{\omega}_x) + \Delta J(\omega_y + \Delta\omega_y)(\omega_z + \Delta\omega_z) = 0$$

$$J_y(\dot{\omega}_y + \Delta\dot{\omega}_y) + (J_x - J_y - \Delta J)(\omega_z + \Delta\omega_z)(\omega_x + \Delta\omega_x) = 0$$

$$(J_y + \Delta J)(\dot{\omega}_z + \Delta\dot{\omega}_z) + (J_y - J_x)(\omega_x + \Delta\omega_x)(\omega_y + \Delta\omega_y) = 0$$

$$\text{where} \quad \Delta J = J_z - J_y$$

Subtracting (4a) from these equations and retaining only the first-order terms gives

$$J_x\Delta\dot{\omega}_x + \Delta J\omega_y\omega_z = 0$$

$$J_y\Delta\dot{\omega}_y - (J_y - J_x)(\omega_z\Delta\omega_x + \omega_x\Delta\omega_z) - \Delta J\omega_x\omega_z = 0$$

$$\Delta J\dot{\omega}_z + J_y\Delta\dot{\omega}_z + (J_y - J_x)(\omega_y\Delta\omega_x + \omega_x\Delta\omega_y) = 0$$

or

$$\Delta\dot{\omega}_x = -\varepsilon_x\omega_y\omega_z$$

$$\Delta\dot{\omega}_y - \Gamma\omega_x\Delta\omega_z - \Gamma\omega_z\Delta\omega_x - \varepsilon_y\omega_x\omega_z = 0$$

$$\Delta\dot{\omega}_z + \Gamma\omega_x\Delta\omega_y + \Gamma\omega_y\Delta\omega_x - \varepsilon_y C\omega_y = 0$$

where

$$\varepsilon_x = \frac{\Delta J}{J_x}, \quad \varepsilon_y = \frac{\Delta J}{J_y}, \quad \Gamma = \frac{J_y - J_x}{J_y} \tag{24}$$

and $\dot{\omega}_z$ is replaced by $-C\omega_y$ as obtained from (4b). The first of the differential equations becomes, from (4d)

$$\Delta\dot{\omega}_x = -\varepsilon_x\left(\omega_{y_0}\omega_{z_0}\cos 2Ct + \frac{\omega_{z_0}^2 - \omega_{y_0}^2}{2}\sin 2Ct\right)$$

which integrates into

$$\Delta\omega_x = E_1\cos 2Ct + E_2\sin 2Ct - E_1 + \Delta\omega_x(0) \tag{25}$$

where

$$E_1 = \frac{\omega_{z_0}^2 - \omega_{y_0}^2}{4C}\varepsilon_x, \quad E_2 = -\frac{\omega_{y_0}\omega_{z_0}}{2C}\varepsilon_x$$

By appropriate use of the imaginary unit, the second and third differential equations become

$$\Delta\dot{\omega}_y + i\Gamma\omega_x i\Delta\omega_z + i\Gamma i\omega_z\Delta\omega_x = \varepsilon_y\omega_x\omega_z$$

$$i\Delta\dot{\omega}_z + i\Gamma\omega_x\Delta\omega_y + i\Gamma\omega_y\Delta\omega_x = i\varepsilon_y C\omega_y$$

Letting

$$\omega = \omega_y + i\omega_z, \quad \Delta\omega = \Delta\omega_y + i\Delta\omega_z$$

addition of the differential equations produces

$$\Delta\dot{\omega} + i\Gamma\Delta\omega_x\Delta\omega + i\Gamma\omega\Delta\omega_x = \varepsilon_y(\omega_x\omega_z + iC\omega_y)$$

or

$$\Delta\dot{\omega} + iC\Delta\omega = -i\Gamma\omega\Delta\omega_x + \varepsilon_y\omega_x(\omega_z + i\Gamma\omega_y) \tag{26}$$

where from (24) and (4c)

$$C = \Gamma\omega_x \tag{27}$$

Multiplying (26) by e^{iCt} gives

$$\frac{d}{dt}(e^{iCt}\,\Delta\omega) = e^{iCt}\left[-i\Gamma\omega\Delta\omega_x + \varepsilon_y\omega_x(\omega_z + i\Gamma\omega_y)\right]$$

which integrates into

$$e^{iCt}\,\Delta\omega = \int_o^t f(\tau)\,d\tau + \Delta\omega(0)$$

where

$$f(\tau) = e^{iCt}\left[-i\Gamma\omega\Delta\omega_x + \varepsilon_y\omega_x(\omega_z + i\Gamma\omega_y)\right]$$

Thus

$$\Delta\omega = e^{-iCt}\left[F(t) + \Delta\omega(0)\right] \tag{28}$$

where

$$F(t) = \int_o^t f(\tau)\,d\tau$$

Letting $F_y(t)$ and $F_z(t)$ denote respectively the real and imaginary parts of F, it follows from (28) that

$$\Delta\omega = (\cos Ct - i\sin Ct)\left\{F_y(t) + \Delta\omega_y(0) + i\left[F_z(t) + \Delta\omega_z(0)\right]\right\}$$

and

$$\Delta\omega_y = \left[F_y(t) + \Delta\omega_y(0)\right]\cos Ct + \left[F_z(t) + \Delta\omega_z(0)\right]\sin Ct$$
$$\Delta\omega_z = -\left[F_y(t) + \Delta\omega_y(0)\right]\sin Ct + \left[F_z(t) + \Delta\omega_z(0)\right]\cos Ct \qquad (29)$$

The formulas (25) and (29) may be substituted into (46) to obtain the perturbed rotation Δp. From (47) (see section 2.2.2.2 following from equations (46) and (47)):

$$p\Delta\bar{\omega}^B p^{-1} = M\Delta\bar{\omega} \qquad (30)$$

where, for the present problem M is to be replaced by P^T where P is given by (4e) and (5) and can be expressed by:

$$P^T = (P_3P_2P_1)^T = P_1^T P_2^T P_3^T \qquad (31)$$

where

$$P_1 = \begin{bmatrix} 1 & 0 & 0 \\ 0 & \cos\theta_1 & \sin\theta_1 \\ 0 & -\sin\theta_1 & \cos\theta_1 \end{bmatrix}$$

$$P_2 = \begin{bmatrix} \cos\theta_2 & 0 & -\sin\theta_2 \\ 0 & 1 & 0 \\ \sin\theta_2 & 0 & \cos\theta_2 \end{bmatrix}$$

$$P_3 = \begin{bmatrix} 1 & 0 & 0 \\ 0 & \cos\theta_3 & \sin\theta_3 \\ 0 & -\sin\theta_3 & \cos\theta_3 \end{bmatrix}$$

Combining (30) and (31) gives

$$p\Delta\bar{\omega}^B p^{-1} = P_1^T P_2^T P_3^T \Delta\bar{\omega}^B \qquad (32)$$

The term $P_3^T \Delta\omega^{-B}$ is to be examined closely. It is shown below that $\dot{\theta}_3$ equals C. From (12a):

$$\dot{\theta}_3 = \frac{H}{J_y} \frac{J_y - J_x}{J_x} \cos\theta_2$$

or

$$\dot{\theta}_3 = \frac{J_y - J_x}{J_y} \frac{H}{J_x} \cos\theta_2.$$

From the first of (9),

$$\omega_x = \frac{H}{J_x} \cos\theta_2$$

Thus

$$\dot{\theta}_3 = \frac{J_y - J_x}{J_y} \omega_x$$

or, from (24) and (27),

$$\dot{\theta}_3 = \Gamma\omega_x = C$$

$$\theta_3 = Ct + \theta_3(0)$$

It was previously assumed in determining θ_3^* that the initial value $\theta_3(0)$ equalled zero. This is valid for a symmetric body since the Y and Z principal axes can be considered to lie anywhere in the YZ-plane. This assumption is not correct for a nonsymmetric body. The calculation of θ_3^* described earlier continues to be valid if θ_3^* is defined to be the final value of θ_3 minus the initial value $\theta_3(0)$.

It is seen from (29) that the multiplication of $F(t) + \Delta\omega(0)$ by e^{-iCt} in (28) is equivalent to a rotation of the Y and Z axes

through the angle Ct about the x-axis. Since P_3^T describes the rotation of θ_3 (equal to Ct + $\theta_3(0)$) about the negative x-axis, it follows that:

$$P_3^T \Delta\bar{\omega}^B = P_3^T(0) \begin{bmatrix} \Delta\omega_x \\ F_y(t) + \Delta\omega_y(0) \\ F_z(t) + \Delta\omega_z(0) \end{bmatrix} \tag{33}$$

where $P_3(0)$ is the initial condition of P_3. By combining (32), (33), and (46)*, the perturbed rotation is obtained as

$$\Delta p = \frac{1}{2} \left\{ \int_o^t P_1^T P_2^T P_3^T(0) \begin{bmatrix} \Delta\omega_x \\ F_y(\tau) + \Delta\omega_y(0) \\ F_z(\tau) + \Delta\omega_z(0) \end{bmatrix} d\tau \right\} p$$

The integrand consists of constants and products of trigonometric functions of Ct, 2Ct, and $\dot{\theta}_1 t$. The integration can therefore be done analytically although it is rather involved.

2.2.2.2 Stability Analysis for Special Case and for Simplified Guidance Law

This section discusses the stability problem using the simplified guidance law where the shuttle is first rotated in roll until its z-axis intersects an extension of the target vehicle docking hatch axis and then simultaneous translation and rotation about the intermediate Y or pitch axis is initiated. The vehicle arrives at an aim point with proper pitch orientation and then is rotated about its x or roll axis to complete the maneuver (This discussion also pertains to the

---

*Equation (46) appears in section 2.2.2.2 following

special case when rotation about the y-axis only is demanded when employing the more sophisticated desired guidance law.).

Rotation about the axis of minimum inertia or of maximum inertia is stable, but rotation about the axis of an intermediate inertia in unstable. These conclusions follow from Euler's equations (4) repeated here (for zero torque)

$$\begin{aligned} J_x\dot{\omega}_x + (J_z - J_y)\omega_y\omega_z &= 0 \\ J_y\dot{\omega}_y + (J_x - J_z)\omega_z\omega_x &= 0 \\ J_z\dot{\omega}_z + (J_y - J_x)\omega_x\omega_y &= 0 \end{aligned} \tag{34}$$

If the initial condtions are

$$\omega_x(0) = \omega_z(0) = 0$$

$$\omega_y(0) \text{ nonzero}$$

then ω_x and ω_z remain zero and ω_y retains its initial condition. Let the reference motion be a constant angular velocity about the y-axis. If this is perturbed by small initial ω_x and ω_z, the resulting angular velocity components are

$$\Delta\omega_x \ , \quad \omega_y + \Delta\omega_y \ , \quad \Delta\omega_z$$

These perturbations are to be determined by a first order analysis. The second equation of (34) becomes

$$J_y(\dot{\omega}_y + \Delta\dot{\omega}_y) + (J_x - J_z)\Delta\omega_z\Delta\omega_y = 0$$

or, to first order,

$$J_y\Delta\dot{\omega}_y = 0$$

from which $\Delta\omega_y$ is constant. The first and third equations of (34) are:

$$J_x\Delta\dot{\omega}_x + (J_z - J_y)(\omega_y + \Delta\omega_y)\Delta\omega_z = 0$$

$$J_z\Delta\dot{\omega}_z + (J_y - J\ )(\omega_y + \Delta\omega_x)\Delta\omega_x = 0$$

or, to first order,

$$\begin{aligned} \Delta\dot{\omega}_x &= \frac{J_y - J_z}{J_x}\omega_y\Delta\omega_z \\ \Delta\dot{\omega}_z &= \frac{J_x - J_y}{J_z}\omega_y\Delta\omega_x \end{aligned} \tag{35}$$

Differentiation and elimination of the first derivatives gives:

$$\begin{aligned} \Delta\ddot{\omega}_x &= \frac{J_y - J_z}{J_x}\frac{J_x - J_y}{J_z}\omega_y^2\Delta\omega_x \\ \Delta\ddot{\omega}_z &= \frac{J_y - J_z}{J_x}\frac{J_x - J_y}{J_z}\omega_y^2\Delta\omega_z \end{aligned} \tag{36}$$

In order that the above equations can be used without change of parameters such that the three conditions of I_y can be studied assume that

(Condition 1) $J_y < J_z < J_x$ or $J_y < J_x < J_z$

so that the reference rotation occurs about the axis of least inertia. Rewriting (36) in terms of positive coefficients,

$$\Delta\ddot{\omega}_x = -\frac{J_z - J_y}{J_x}\frac{J_x - J_y}{J_z}\omega_y^2\Delta\omega_x$$

$$\Delta\ddot{\omega}_z = -\frac{J_z - J_y}{J_x}\frac{J_x - J_y}{J_z}\omega_y^2\Delta\omega_z$$

and the angular velocity perturbations are sinusoidal and bounded. Next assume that

(Condition 2) $J_z < J_x < J_y$ or $J_x < J_z < J_y$

so that the rotation occurs about the axis of greatest inertia. Then

then

$$\Delta\ddot{\omega}_x = -\frac{J_y - J_z}{J_x}\frac{J_y - J_x}{J_z}\omega_y^2\Delta\omega_x$$

$$\Delta\ddot{\omega}_z = -\frac{J_y - J_z}{J_x}\frac{J_y - J_x}{J_z}\omega_y^2\Delta\omega_z$$

and here also the perturbations are sinusoidal. Now assume that

(Condition 3a) $$J_z < J_y < J_x$$

so that the rotation occurs about the axis of intermediate inertia. Then the coefficients in (36) are positive and the angular velocity perturbations are exponential and unbounded. Similarly for the case of the SSV studied

(Condition 3b) $$J_x < J_y < J_z$$

then

$$\Delta\ddot{\omega}_x = K_x K_z \omega_y^2 \Delta\omega_x$$

$$\Delta\ddot{\omega}_z = K_x K_z \omega_y^2 \Delta\omega_z \qquad (37)$$

where

$$K_x = \frac{J_z - J_y}{J_x} > 0$$

$$K_z = \frac{J_y - J_x}{J_z} > 0 \qquad (38)$$

The specific question that occurred concerned the possibility of the shuttle pitching about its y-axis (the axis of intermediate inertia) and it is this case which is analyzed below.

Let

$$\kappa = \sqrt{K_x K_z}\,\omega_y \qquad (39)$$

then (37) and (35) become

$$\Delta\ddot{\omega}_x = \kappa^2 \Delta\omega_x$$
$$\Delta\ddot{\omega}_z = \kappa^2 \Delta\omega_z \tag{40}$$

and

$$\Delta\dot{\omega}_x = -\kappa_x \omega_y \Delta\omega_x$$
$$\Delta\dot{\omega}_z = -\kappa_z \omega_y \Delta\omega_x \tag{41}$$

The solution of (40) is

$$\Delta\omega_x = \Delta\omega_x(0)\cosh\kappa t + \frac{1}{\kappa}\Delta\dot{\omega}_x(0)\sinh\kappa t$$
$$\Delta\omega_z = \Delta\omega_z(0)\cosh\kappa t + \frac{1}{\kappa}\Delta\dot{\omega}_z(0)\sinh\kappa t$$

The initial values of the derivatives are available from (41), and

$$\Delta\omega_x = \Delta\omega_x(0)\cosh\kappa t - \sqrt{K_x/K_z}\,\Delta\omega_z(0)\sinh\kappa t$$
$$\Delta\omega_z = \Delta\omega_z(0)\cosh\kappa t - \sqrt{K_z/K_x}\,\Delta\omega_x(0)\sinh\kappa t \tag{42}$$

These are the angular velocity perturbations caused by initial deviations. The equations are valid for small values of $\Delta\omega_x$ and $\Delta\omega_z$ whereby second and higher order terms may be neglected.

The next task is to solve a differential equation for the perturbation of the resultant rotation from the reference rotation occurring about the shuttle's y-axis. A convenient equation is

$$\dot{p} = \frac{1}{2} p \bar{\omega}^B \tag{43}$$

where p is the quaternion of rotation defined as

$$p = \lambda + \bar{\rho} \tag{44}$$

and

$$\lambda = \cos\frac{\theta}{2}$$
$$\bar{\rho} = \bar{n}\sin\frac{\theta}{2}$$

where $\bar{n}$ is the unit vector along the axis of rotation from the shuttle's initial orientation to its orientation at time t and θ (measured about $\bar{n}$) is the angle between the two orientations. Here $\bar{\omega}^{B}$ denotes specifically the body's components of $\bar{\omega}$ and $\dot{p}$ is the derivative of p with respect to the body's axis frame. The perturbed equation is

$$\Delta\dot{p} = \frac{1}{2}(\Delta p\bar{\omega}^{B} + p\Delta\bar{\omega}^{B})$$

or

$$\Delta\dot{p} - \frac{1}{2}\Delta p\bar{\omega}^{B} = \frac{1}{2}p\Delta\bar{\omega}^{B} \tag{45}$$

where the components of $\Delta\bar{\omega}^{B}$ are given by (42). Solving (43) for $\bar{\omega}^{B}$ gives

$$\bar{\omega}^{B} = 2p^{-1}\dot{p}$$

Since

$$p^{-1}p = 1$$

this is equivalent to

$$\bar{\omega}^{B} = -2\frac{dp^{-1}}{dt}$$

and substitution into (45) gives

$$\Delta\dot{p} + \Delta p\frac{dp^{-1}}{dt}p = \frac{1}{2}p\Delta\bar{\omega}^{B}$$

Multiplying on the right by p^{-1},

$$\Delta\dot{p}p^{-1} + \Delta p\frac{dp^{-1}}{dt} = \frac{1}{2}p\Delta\bar{\omega}^{B}p^{-1}$$

or

$$\frac{d}{dt}(\Delta p p^{-1}) = \frac{1}{2} p \Delta\bar{\omega}^{-B} p^{-1}$$

This integrates into

$$\Delta p p^{-1} = \frac{1}{2}\int_o^t p \Delta\bar{\omega}^{-B} p^{-1} d\tau$$

and

$$\Delta p = \frac{1}{2}\left[\int_o^t p \Delta\bar{\omega}^{-B} p^{-1} d\tau\right] p \tag{46}$$

The integrand is the transformation from the body components of $\Delta\bar{\omega}$ to the inertial components,

$$p \Delta\bar{\omega}^{-B} p^{-1} = M \Delta\bar{\omega}^{-B} \tag{47}$$

where

$$M = \begin{bmatrix} \cos\omega_y\tau & 0 & \sin\omega_y\tau \\ 0 & 1 & 0 \\ -\sin\omega_y\tau & 0 & \cos\omega_y\tau \end{bmatrix}$$

Then, from (42),

$$\begin{aligned} p \Delta\bar{\omega}^{-B} p^{-1} = {} & \left[\Delta\omega_x(0)\cosh\kappa\tau\cos\omega_y\tau - \sqrt{K_x/K_z}\,\Delta\omega_z(0)\sinh\kappa\tau\cos\omega_y\tau\right. \\ & \left. - \sqrt{K_z/K_x}\,\Delta\omega_x(0)\sinh\kappa\tau\sin\omega_y\tau + \Delta\omega_z(0)\cosh\kappa\tau\sin\omega_y\tau\right]\bar{i} \\ & + \left[-\Delta\omega_x(0)\cosh\kappa\tau\sin\omega_y\tau + \sqrt{K_x/K_x}\,\Delta\omega_z(0)\sinh\kappa\tau\sin\omega_y\tau\right. \\ & \left. - \sqrt{K_z/K_x}\,\Delta\omega_x(0)\sinh\kappa\tau\cos\omega_y\tau + \Delta\omega_z(0)\cosh\kappa\tau\cos\omega_y\tau\right]\bar{k} \end{aligned}$$

Each component is a linear combination of

$$\cosh\kappa\tau\cos\omega_y\tau$$

$$\cosh\kappa\tau\sin\omega_y\tau$$

$$\sinh\kappa\tau\cos\omega_y\tau$$

$$\sinh\kappa\tau\sin\omega_y\tau$$

It is next shown that the integral of such a combination is likewise a linear combination of the same functions. Let

$$F = A_{11}\cosh\kappa\tau\cos\omega_y\tau + A_{12}\cosh\kappa\tau\sin\omega_y\tau + A_{21}\sinh\kappa\tau\cos\omega_y\tau + A_{22}\sinh\kappa\tau\sin\omega_y\tau$$

where the A_{ij} are arbitrary constants. Then

$$\frac{dF}{d\tau} = A_{11}(\kappa\sinh\kappa\tau\cos\omega_y\tau - \omega_y\cosh\kappa\tau\sin\omega_y\tau) + A_{12}(\kappa\sinh\kappa\tau\sin\omega_y\tau + \omega_y\cosh\kappa\tau\cos\omega_y\tau) + A_{21}(\kappa\cosh\kappa\tau\cos\omega_y\tau - \omega_y\sinh\kappa\tau\sin\omega_y\tau) + A_{22}(\kappa\cosh\kappa\tau\sin\omega_y\tau + \omega_y\sinh\kappa\tau\cos\omega_y\tau)$$

or

$$\frac{dF}{d\tau} = B_{11}\cosh\kappa\tau\cos\omega_y\tau + B_{12}\cosh\kappa\tau\sin\omega_y\tau + B_{21}\sinh\kappa\tau\cos\omega_y\tau + B_{22}\sinh\kappa\tau\sin\omega_y\tau$$

where

$$B_{11} = \omega_y A_{12} + \kappa A_{21}$$

$$B_{12} = -\omega_y A_{11} + \kappa A_{22}$$

$$B_{21} = \kappa A_{11} + \omega_y A_{22}$$

$$B_{22} = \kappa A_{12} - \omega_y A_{21}$$

If the B_{ij} are given (as in the present problem), the A_{ij} are obtained as

$$A_{11} = \frac{\kappa B_{21} - \omega_y B_{12}}{\kappa^2 + \omega_y^2}$$

$$A_{12} = \frac{\kappa B_{22} + \omega_y B_{11}}{\kappa^2 + \omega_y^2}$$

$$A_{21} = \frac{\kappa B_{11} - \omega_y B_{22}}{\kappa^2 + \omega_y^2}$$

$$A_{22} = \frac{\kappa B_{12} + \omega_y B_{21}}{\kappa^2 + \omega_y^2}$$

Letting

$$\bar{F} = F_x \bar{i} + F_z \bar{k} = \int_o^t p \Delta\omega^{-B} p^{-1} d_\tau$$

it is seen from the preceding formulas that

$$F_x = A_{11}\cosh\kappa t \cos\omega_y t + A_{12}\cosh\kappa t \sin\omega_y t$$

$$+ A_{21}\sinh\kappa t \cos\omega_y t + A_{22}\sinh\kappa t \sin\omega_y t - A_{11}$$

where

$$A_{11} = \frac{-\kappa\sqrt{K_x/K_z}\,\Delta\omega_z(0) - \omega_y \Delta\omega_z(0)}{\kappa^2 + \omega_y^2} = -\frac{J_z}{J_y}\frac{\Delta\omega_z(0)}{\omega_y}$$

$$A_{12} = \frac{-\kappa\sqrt{K_z/K_x}\,\Delta\omega_x(0) + \omega_y\Delta\omega_x(0)}{\kappa^2 + \omega_y^2} = \frac{J_x}{J_y}\,\frac{\Delta\omega_x(0)}{\omega_y}$$

$$A_{21} = \frac{\kappa\Delta\omega_x(0) + \omega_y\sqrt{K_z/K_x}\,\Delta\omega_x(0)}{\kappa^2 + \omega_y^2} = \frac{J_z}{J_y}\sqrt{\frac{K_z}{K_x}}\,\frac{\Delta\omega_x(0)}{\omega_y}$$

$$A_{22} = \frac{\kappa\Delta\omega_z(0) - \omega_y\sqrt{K_x/K_z}\,\Delta\omega_z(0)}{\kappa^2 + \omega_y^2} = -\frac{J_x}{J_y}\sqrt{\frac{K_x}{K_2}}\,\frac{\Delta\omega_z(0)}{\omega_y}$$

Similarly

$$F_z = C_{11}\cosh\kappa t\cos\omega_y t + C_{12}\cosh\kappa t\sin\omega_y t + C_{21}\sinh\kappa t\cos\omega_y t + C_{22}\sinh\kappa t\sin\omega_y t - C_{11}$$

where

$$C_{11} = \frac{-\kappa\sqrt{K_z/K_x}\,\Delta\omega_x(0) + \omega_y\Delta\omega_x(0)}{\kappa^2 + \omega_y^2} = A_{12}$$

$$C_{12} = \frac{\kappa\sqrt{K_x/K_z}\,\Delta\omega_z(0) + \omega_y\Delta\omega_z(0)}{\kappa^2 + \omega_y^2} = -A_{11}$$

$$C_{21} = \frac{\kappa\Delta\omega_z(0) - \omega_y\sqrt{K_x/K_z}\,\Delta\omega_z(0)}{\kappa^2 + \omega_y^2} = A_{22}$$

$$C_{22} = \frac{-\kappa\Delta\omega_x(0) - \omega_y\sqrt{K_z/K_x}\,\Delta\omega_x(0)}{\kappa^2 + \omega_y^2} = -A_{21}$$

so that

$$F_z = A_{12}\cosh\kappa t\cos\omega_y t - A_{11}\cosh\kappa\tau\sin\omega_y\tau + A_{22}\kappa\sinh\kappa t\cos\omega_y t - A_{21}\sinh\kappa\tau\sin\omega_y\tau - A_{12}$$

Finally, from (46) and (44)

$$\Delta p = \frac{1}{2}\bar{F}(\lambda + \rho\bar{j})$$

or

$$\Delta p = \frac{1}{2}(\lambda\bar{F} + \bar{F} \times \bar{j})$$

and

$$\Delta p = \frac{1}{2}\left[\lambda(F_x\bar{i} + F_z\bar{k}) + \rho(F_x\bar{k} - F_z\bar{i})\right]$$

or

$$\Delta p = \frac{1}{2}\left[(\lambda F_x - \rho F_z)\bar{i} + (\lambda F_z + \rho F_x)\bar{k}\right]$$

Substituting for λ and ρ in terms of $\omega_y t$,

$$\Delta p = \frac{1}{2}\left[(F_x\cos\frac{\omega_y t}{2} - F_z\sin\frac{\omega_y t}{2})\bar{i} + (F_x\sin\frac{\omega_y t}{2} + F_z\cos\frac{\omega_y t}{2})\bar{k}\right]$$

This equation becomes somewhat involved when the formulas for F_x and F_z are substituted into it. A simplification follows. In matrix-vector form

$$\Delta p = \frac{1}{2}M_1\bar{F} \qquad (48)$$

where

$$M_1 = \begin{bmatrix} \cos\frac{\omega_y t}{2} & -\sin\frac{\omega_y t}{2} \\ \sin\frac{\omega_y t}{2} & \cos\frac{\omega_y t}{2} \end{bmatrix}$$

The components F_x and F_z can themselves be expressed in terms of another vector $\bar{G}$,

$$\bar{F} = M_2\bar{G} - \bar{A} \tag{49}$$

where

$$M_2 = \begin{bmatrix} \cos\omega_y t & \sin\omega_y t \\ -\sin\omega_y t & \cos\omega_y t \end{bmatrix}$$

$$\bar{A} = \begin{bmatrix} A_{11} \\ A_{12} \end{bmatrix}$$

$$\bar{G} = \begin{bmatrix} G_x \\ G_z \end{bmatrix}$$

$$G_x = A_{11}\cosh\kappa t + A_{21}\sinh\kappa t$$

$$G_z = A_{12}\cosh\kappa t + A_{22}\sinh\kappa t$$

Substituting (49) into (48)

$$\Delta p = \frac{1}{2}(M_1M_2\bar{G} - M_1\bar{A})$$

which becomes

$$p = \frac{1}{2}\begin{bmatrix} \cos\frac{\omega_y t}{2} & \sin\frac{\omega_y t}{2} \\ -\sin\frac{\omega_y t}{2} & \cos\frac{\omega_y t}{2} \end{bmatrix}\begin{bmatrix} G_x \\ G_z \end{bmatrix} - \frac{1}{2}\begin{bmatrix} \cos\frac{\omega_y t}{2} & -\sin\frac{\omega_y t}{2} \\ \sin\frac{\omega_y t}{2} & \cos\frac{\omega_y t}{2} \end{bmatrix}\begin{bmatrix} A_{11} \\ A_{12} \end{bmatrix}$$

Then

$$\Delta p_x = \frac{1}{2}\,(G_x - A_{11})\cos\frac{\omega_y t}{2} + (G_z + A_{12})\sin\frac{\omega_y t}{2}$$

$$\Delta p_z = \frac{1}{2}\;-(G_x + A_{11})\sin\frac{\omega_y t}{2} + (G_z - A_{12})\cos\frac{\omega_y t}{2}$$

2.2.3 Autopilot, Propulsion, and Vehicle Effects

MIT has conceived a jet selection logic program for use with the autopilot which could be used on the SSV. This program is proposed for operation during several phases of the SSV mission including the docking operation.

Because of the special nature of the guidance law, the thresholding of engine (RCS) firings might well be accomplished by the guidance computer. This problem should be reviewed in later studies.

2.2.4 Orbital Disturbances and Effects

Two point masses in separate orbits have relative dynamics which exist between them because of the presence of the gravitational field. An approximate expression for the orbital mechanics involved is:

$$\ddot{\bar{r}} = ER^{-2}\; 3\bar{\mu}\left(\bar{\mu} \cdot \frac{\bar{r}}{R}\right) + \bar{a}_T$$

where,

$\bar{r}$ relative position (subject-sensor)

$\bar{\ }$ unit vector (earth center to either vehicle)

R distance (earth center to either vehicle)

$\bar{a}_T$ thrust acceleration

E earth's gravitational constant

This equation has an accuracy of 1 part in 10^4 and appears to be sufficiently accurate for incorporation into box (8) of Figure 5.

2.2.5 Geometry Update Solutions

The effects of the guidance outputs, autopilot, vehicle, and engine outputs and orbital disturbance effects should be utilized in the geometry update equations, box (1), figure 5 to close the simulation loop. Completion of the programming of this and the preceding would provide the capability for evaluation of the performance of the angle only and other docking sensor configurations.

2.3 Kalman Filtering Assessment

During the course of this program two approaches to determine the enhancement Kalman filtering provided to the basic docking sensor data were employed.

The first which was reported in the Summary and Current Status Report, dated December 9, 1970 is included herein for completeness:

Let $\bar{X}$ be the estimated state vector

and $\overset{*}{E}$ the correlation matrix of uncertainty in the state vector

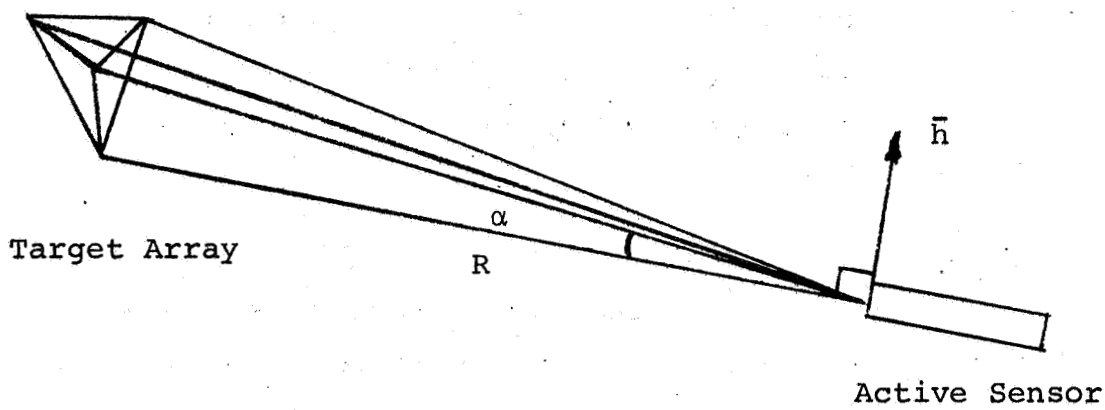

Figure 14. Geometry for Kalman Filter Study.

α is angle measured between two target courses

$\bar{h}$ is a unit vector in plane of measurement perpendicular to one line-of-sight

R is range to target

The measurement update equations are

$$\bar{X}' = X + \frac{\overset{*}{E}\,\bar{b}(\alpha - \beta)}{\bar{b} \cdot E\,\bar{b} + \sigma_m^2}$$

and

$$\overset{*}{E}' = \overset{*}{E} - \frac{(\overset{*}{E}\,\bar{b})(\overset{*}{E}\,\bar{b})^T}{\bar{b} \cdot \overset{*}{E}\,\bar{b} + \sigma_m^2}$$

where

X', E' = new estimate of state and uncertainty

β = angle calculated assuming old $\bar{X}$

σ_m = instrument measurement accuracy

$\bar{b}$ = $\bar{h}/R$

The procedure employed was to start with $\overset{*}{E}$ large enough to represent a priori knowledge of $\bar{X}$ and to update $\bar{X}$ and $\overset{*}{E}$ once for each angle that can be measured. The resulting $\overset{*}{E}$ matrix represents the accuracy to which a sensor of accuracy σ_m can fix the position under the given geometry. The 1σ uncertainty in any direction $\bar{\mu}$ (such as range or elevation set) can be found by solution of the following equation:

$$\sigma_\mu = \sqrt{(\bar{\mu}\,\overset{*}{E}) \cdot \bar{\mu}}$$

Results of this analysis indicate marked improvements in position (and other) knowledge can be achieved as a result of employing estimation techniques for docking. See Table 2 for the presentation of the computed values of position and velocity uncertainties with Kalman filtering employed.

Section 2.1 shows simulation results of position accuracy without the benefit of filtering.

The second study, also previously reported, developed linearized equations around a nominal state consisting of

1. Zero angular misalignment between sensor axes and target (inertial) axes.

TABLE 2

Position and Velocity Uncertainties

- Measurement accuracy 1 arc min
- One independent measurement per second
- Optical target perfect
- ΔV application and measurement perfect

RANGE	POSITION SIGMA		VELOCITY SIGMA	
	= LOS	LOS	= LOS	LOS
200 ft	10 ft	0.5 ft	0.2 FPS	0.01 FPS
10	0.01	0.001*	0.001*	<0.001**
1	0.001*	<0.001*	<0.001**	<0.001**

* Limited by optical properties of target and sensor to ~0.001 ft

** Limited by ΔV application and measurement to ~0.002 FPS

2. Zero angular rate between sensor and target axes.
3. Zero relative linear velocity.
4. Relative position vector having only the x-component non-zero.

The target was in a 150 n mile orbit about a spherical Earth, and was in a perfect inertial attitude hold, with the x-axis out of plane and the z-axis initially up. No thrusting or limit cycling was assumed. A complete measurement incorporation (azimuth and elevation for three target lights) was made every 1/2 second, and a total of ten complete incorporations were made at each value of range in a given set of runs. The target axis was assumed to be centered at light #1. The state vector for the problem consists of the relative linear position and velocity of the body with respect to the target and the relative angular position and velocity of the body with respect to the target, all expressed in body coordinates.

The results indicate that the linear filtering technique predicts rms errors significantly lower than those obtained using the alternate deterministic method. The extremely small errors at ranges less than 50 ft, although not to be entirely trusted, do indicate the power of the measurements at these ranges and indicate that linear filtering techniques will lead to a successful docking. Of particular importance is the good linear position and velocity information perpendicular to the line-of-sight at large ranges. This should allow efficient velocity corrections to be made early in the mission to keep the vehicle within the operating cone. An added advantage of the filtering technique is that it has at all times the (predicted) covariance matrix of estimation errors. This information would be of particular value to an outer loop which must decide

when to alter the velocity along the line-of-sight.

Results of this study are presented in tables 3, 4, and 5. The parameters (position, velocity, attitude, and attitude rate) are calculated and are based upon estimates of the line-of-sight angles to the individual targets. Table 3 presents results that are comparable to the calculated results shown in Table 1 section 2.1) where raw sensor data was used as a basis of computation. The results shown in table 1 are based upon a single measurement whereas the results employing estimation techniques are rms values.

A comparison of tables 4 and 5 show the improvement in estimation realizable with tighter initial conditions. Again the positional cross track uncertainties are small in comparison to the track uncertainties at long ranges and indicate lateral control is effective regardless.

TABLE 3

Tabulation of Results Employing Kalman Filtering
to Angle Only Sensor Data

Initial Conditions: Position (20, 5, 5) Feet
Velocity (5, 1, 1) Feet/Second
Angle (3, 3, 3) Degrees
Angle Rate (0.71, 0.71, 0.71) Degrees/Second

With 10 Measurements at 1/2 Second Intervals Each Reading, Triangle R_1, R_3, R_4 Used.

RANGE	POSITION ERROR FEET			VELOCITY ERROR FEET/SEC			ANGLE ERROR DEGREES			ANGLE RATE ERROR DEGREES/SEC		
	X	Y	Z	$\dot{X}$	$\dot{Y}$	$\dot{Z}$	θ_x	θ_y	θ_z	$\dot{\theta}_x$	$\dot{\theta}_y$	$\dot{\theta}_z$
295	12.6	0.0403	0.0405	3.15	0.0135	0.0135	2.28	2.34	3.41	0.516	0.534	0.536
275	11.4	0.0380	0.0381	2.95	0.0127	0.0128	2.18	2.25	2.32	0.505	0.514	0.530
255	10.2	0.0356	0.0357	2.72	0.0120	0.0120	2.08	2.14	2.22	0.493	0.502	0.523
235	8.92	0.0331	0.0333	2.48	0.0112	0.0112	1.98	2.04	2.11	0.480	0.489	0.515
215	7.72	0.0306	0.0308	2.22	0.0104	0.0105	1.86	1.92	1.99	0.466	0.475	0.506
195	6.55	0.0280	0.0282	1.95	0.0095	0.0096	1.74	1.79	1.87	0.450	0.459	0.495
175	5.43	0.0354	0.0256	1.67	0.0087	0.0088	1.61	1.66	1.73	0.432	0.442	0.481
155	4.37	0.0227	0.0229	1.39	0.0078	0.0080	1.47	1.52	1.59	0.411	0.421	0.462
135	3.41	0.0200	0.0202	1.12	0.0070	0.0071	1.33	1.37	1.43	0.387	0.398	0.438
115	2.53	0.0172	0.0174	0.856	0.0061	0.0061	1.17	1.21	1.26	0.359	0.369	0.406
95	1.76	0.0144	0.0144	0.613	0.0051	0.0052	1.01	1.04	1.08	0.324	0.333	0.363
75	1.11	0.0114	0.0114	0.396	0.0041	0.0042	0.825	0.850	0.875	0.279	0.287	0.306
55	0.590	0.0083	0.0083	0.216	0.0031	0.0031	0.622	0.640	0.648	0.220	0.226	0.234
35	0.225	0.0051	0.0051	0.0835	0.0019	0.0019	0.393	0.403	0.398	0.144	0.148	0.147
15	0.0297	0.0017	0.0017	0.0111	0.0006	0.0006	0.140	0.142	0.132	0.0524	0.0529	0.0494
10	0.0177	0.0009	0.0009	0.0066	0.0003	0.0003	0.173	0.166	0.175	0.0644	0.0619	0.0654
8	0.0072	0.0005	0.0005	0.0027	0.0002	0.0002	0.108	0.0985	0.108	0.0403	0.0369	0.0404
6.5	0.0024	0.0003	0.0003	0.0009	0.0001	0.0001	0.0595	0.0493	0.0582	0.0223	0.0185	0.0218
6.0	0.0013	0.0002	0.0002	0.0005	0.0001	0.0001	0.0437	0.0338	0.0422	0.0164	0.0127	0.0158
5.5	0.0006	0.0001	0.0001	0.0002	0.0000	0.0000	0.0286	0.0199	0.0272	0.0107	0.00745	0.0102
5.2	0.0003	0.0000	0.0000	0.0001	0.0000	0.0000	0.0206	0.0135	0.0196	0.0077	0.00505	0.00735

TABLE 4

Results Employing Kalman Filtering with Large Initial Uncertainties
Initial Conditions: Position (100, 100, 100) Feet
Velocity (10, 10, 10) Feet/Second
Angle (10, 10, 10) Degrees
Angle Rate (1, 1, 1) Degrees/Second
10 Measurements at 1/2 Second Intervals Each Reading, Triangle R_1, R_3, R_4

RANGE	POSITION UNCERTAINTY FEET			VELOCITY UNCERTAINTY FEET/SECOND			ANGLE UNCERTAINTY DEGREES			ANGLE RATE UNCERTAINTY DEGREES/SECOND		
	X	Y	Z	$\dot{X}$	$\dot{Y}$	$\dot{Z}$	θX	θY	θZ	$\dot{\theta} X$	$\dot{\theta} Y$	$\dot{\theta} Z$
1000	82.1	0.123	0.123	9.64	0.0400	0.4030	5.98	6.15	5.58	0.917	0.922	0.917
900	74.8	0.112	0.113	9.51	0.0366	0.0368	5.65	5.81	5.41	0.906	0.911	0.906
800	66.1	0.102	0.102	9.33	0.0332	0.0334	5.28	5.43	5.19	0.891	0.897	0.892
700	56.2	0.0911	0.0912	9.04	0.0298	0.0299	4.86	5.01	4.89	0.872	0.879	0.875
600	45.6	0.0800	0.0500	8.58	0.0263	0.0264	4.39	4.53	4.50	0.848	0.856	0.854
500	35.0	0.0685	0.0685	7.80	0.0228	0.0228	3.88	3.99	4.02	0.814	0.825	0.831
400	24.9	0.0565	0.0566	6.55	0.0191	0.0191	3.30	3.41	3.46	0.769	0.782	0.808
300	15.7	0.0438	0.0441	4.75	0.0151	0.0152	2.68	2.76	2.85	0.706	0.721	0.776
200	7.88	0.0306	0.0308	2.65	0.0108	0.1090	2.00	2.06	2.16	0.607	0.624	0.689
100	2.24	0.0163	0.0164	0.815	0.0060	0.0060	1.18	1.22	1.26	0.414	0.427	0.452

TABLE 5

Results Employing Kalman Filtering with Small Initial uncertainties
Initial Conditions: Position (5, 5, 5) Feet
Velocity (0.316, 0.316, 0.316) Feet/Second
Angle (10, 10, 10) Degrees
Angle Rate (1, 1, 1) Degrees/Second
10 Measurements at 1/2 Second Intervals Each Reading, Triangle Used R_1, R_3, R_4

RANGE	POSITION UNCERTAINTY FEET			VELOCITY UNCERTAINTY FEET/SECOND			ANGLE UNCERTAINTY DEGREES			ANGLE RATE UNCER DEGREES/SECOND		
	X	Y	Z	$\dot{X}$	$\dot{Y}$	$\dot{Z}$	θ_x	θ_y	θ_z	$\dot{\theta}_x$	$\dot{\theta}_x$	$\dot{\theta}_y$
1000	5.24	0.122	0.121	0.316	0.0395	0.0399	5.98	6.15	4.33	0.917	0.921	0.911
900	5.24	0.111	0.110	0.316	0.036	0.0365	5.64	5.81	4.02	0.906	0.911	0.898
800	5.23	0.100	0.100	0.316	0.033	0.033	5.28	5.43	3.69	0.891	0.897	0.882
700	5.22	0.089	0.089	0.316	0.029	0.030	4.86	5.00	3.37	0.872	0.879	0.859
600	5.21	0.0778	0.0777	0.316	0.0258	0.0261	4.39	4.52	3.04	0.847	0.855	0.828
500	5.17	0.0665	0.0663	0.316	0.0224	0.0225	3.87	3.99	2.69	0.814	0.824	0.784
400	5.08	0.0549	0.0546	0.316	0.0188	0.0187	3.30	3.40	2.35	0.769	0.781	0.719
300	4.78	0.0429	0.0424	0.315	0.015	0.0147	2.68	2.76	1.99	0.706	0.721	0.620
200	3.72	0.0301	0.0296	0.312	0.0107	0.0105	2.00	2.06	1.61	0.607	0.623	0.473
100	1.43	0.016	0.016	0.016	0.291	0.058	1.18	0.22	0.982	0.414	0.427	0.291

3.0 Conclusions and Recommendations

This study program has proven the functional feasibility of utilizing an angle only sensor; operating in cooperation with a target array of known physical dimensions, mounted on a passive vehicle; during the automatic docking of large spacecraft. A parametric analysis is required to optimize the sensor/target configuration to ascertain such factors as sensor field-of-view scale change requirements, operating wavelength, target size and configuration, and other parameters for utilization during the docking mission. Effects of the operating limits for the sensor, the profile, vehicle configuration, background condition, and other factors should be reflected in the final sensor subsystem design. Benefits derived from Kalman estimation techniques were investigated during the study. The results show considerable promise for the utilization of these techniques where the angle only sensor concept is employed.

A computer simulation program was conceived and partially implemented. The overall program was intended to simulate the complete automatic docking process from a given set of initial conditions to actual hard dock taking into account sensor performance, the guidance law, the active vehicle autopilot configuration, the vehicle response characteristics, and the orbital effects-all in closed loop simulation. It was intended that provision for the evaluation of several types of sensors be incorporated into the simulation.

Unfortunately the complete simulation was never accomplished because of the lack of availability of valid guidance equations until near the end of this program. Derivation of the guidance equations which provide commands for simultaneous control of

active vehicle translation and rotation which minimizes Δv consumption and allows the docking maneuver to be performed safely and in a minimum amount of time was accomplished. Several alternative schemes for the guidance law were considered during the course of the study. Equations for two alternative guidance methods and a related stability analysis are presented herein. Further information regarding the vehicle characteristics and control configuration, and the desired docking profile(s) are necessary before firm guidance law parameters can be established.

It is recommended that the computer simulation be completed in any future effort. A closed loop program would be an extremely useful tool for further analysis where many sets of sensor and system parameters must be examined. Such a tool, with proper variables, can be used to verify the performance of many different sensors with many autopilot and vehicle configurations under varied environments and with different guidance laws. Kalman filtering and other enhancement techniques should be included in the simulation because of the high accuracy that the docking of large space vehicles requires.

Insofar as the guidance equations as discussed herein are concerned, it is recommended that future effort include:

1. a comparison of the perturbed solution with the numerical solution of the exact (Euler's) equations for accuracy and number of solutions,

2. devising a definition of the "best" solution (when two or more exist),

3. an examination of the effect of gravitational torque on the shuttle,

4. an examination of the effect of rotation of the space station.

During this study it was assumed that the SSV onboard computer capacity was sufficient to adequately accomplish the docking operation. Inasmuch as the quidance equations were not developed until the end of the study, computer sizing was not accomplished. It is recommended computer requirements and sizing be accomplished in any future study.

Finally it is recommended that the several sensor subsystems under consideration for automatic docking be evaluated and the better candidates be designed for the specific mission and equipment. It is only after the sensing equipment has been fabricated, calibrated, and tested that enough will be known to adequately implement its parameters into the computer simulation.